

Typical relaxation of perturbed quantum many-body systems

Lennart Dabelow* and Peter Reimann†

Fakultät für Physik, Universität Bielefeld, 33615 Bielefeld, Germany

(Dated: January 12, 2021)

We substantially extend our relaxation theory for perturbed many-body quantum systems from [Phys. Rev. Lett. **124**, 120602 (2020)] by establishing an analytical prediction for the time-dependent observable expectation values which depends on only two characteristic parameters of the perturbation operator: its overall strength and its range or band width. Compared to the previous theory, a significantly larger range of perturbation strengths is covered. The results are obtained within a typicality framework by solving the pertinent random matrix problem exactly for a certain class of banded perturbations and by demonstrating the (approximative) universality of these solutions, which allows us to adopt them to considerably more general classes of perturbations. We also verify the prediction by comparison with several numerical examples.

I. INTRODUCTION

The question of how the behavior of a given system changes in response to a weak perturbation is ubiquitous in physics. If many degrees of freedom are involved, the microscopic dynamics is commonly expected to be extremely sensitive against small changes (chaotic [1]), so that it is virtually impossible to theoretically predict the response exactly or in terms of well-controlled approximations [2]. Yet, the actually observed behavior in experiments and numerical simulations is often found to obey relatively simple and robust “laws”. Here, we specifically ask how the temporal relaxation of an isolated many-body quantum system is altered by a small modification of the Hamiltonian, and we bridge the inevitable gap between what is theoretically feasible and what is actually observed by adopting the general framework of random matrix theory [1, 3].

As our starting point we utilize the tools and results which we previously established in Ref. [4] and summarize here in Sec. II (see also [5–7] for some related earlier works and Sec. VI for a more detailed discussion of their connection to our present approach): Essentially, the idea is to consider not one specific but rather an entire ensemble of perturbations, most of which still closely resemble the one of actual interest. The first main result obtained in Ref. [4] was an analytical prediction for the ensemble-averaged, time-dependent deviations of the perturbed from the unperturbed expectation values of generic observables. In a second step, it was shown that nearly all members of the ensemble behave very similarly to the average. Finally, it was argued that also the system of actual interest belongs to that vast majority. In the context of random matrix theory, this is a well-established line of reasoning, which has to our knowledge never been rigorously justified, but is extremely successful in practice [3]. In fact, it has been originally devised by Wigner for the very purpose of exploring chaotic quan-

tum many-body systems and is by now widely recognized as a remarkably effective tool in this context [1]. We emphasize once more that such an approach should *not* be viewed as a randomization of the real physical perturbation [8, 9]. Rather, the basic assertion is that the “true” (non-random) perturbation belongs to the vast majority of all the very similarly behaving members of some properly chosen ensemble.

Technically speaking, a key role in the above described approach from Ref. [4] is played by a non-linear integral equation, which so far could only be tackled analytically in two limiting cases. At the focus of our present paper is a much more detailed analytical investigation of this non-linear integral equation (Sec. IV).

The central results of this work are summarized in Sec. III and established in detail in Sec. V. Our first main result is that a very large class of perturbations can be extremely well characterized by only two parameters. One of them essentially describes the perturbation strength. The other one quantifies the range of the perturbation in terms of how quickly its matrix elements in the unperturbed eigenbasis decay with their energy difference. Our second main result is a very general analytical approximation of the perturbed relaxation in terms of these two parameters. As a validation of the adopted random matrix approach itself and of our analytical approximations within such an approach, we finally compare our predictions with numerically obtained results for various specific models (Sec. VII). Altogether, notable analytical progress is thus achieved with regard to the general topics of equilibration and thermalization in isolated many-body quantum systems, which are attracting increasing theoretical and experimental interest during recent years, as reviewed, e.g., in Refs. [10–16].

II. SETTING THE STAGE

In this section, we outline the general framework and the main results from the pertinent predecessor work [4], which in turn is very similar in its general spirit to the hallmark paper by Deutsch [5] and its further developments for instance in Refs. [6, 7, 17, 18].

*Electronic address: ldabelow@physik.uni-bielefeld.de

†Electronic address: reimann@physik.uni-bielefeld.de

As announced in the Introduction, we study the temporal relaxation of an isolated many-body quantum system with Hamiltonian

$$H = H_0 + \lambda V, \quad (1)$$

where H_0 describes the unperturbed system, V the perturbation, and λ the coupling. At time $t = 0$, the system is prepared in some pure or mixed, and generally far-from-equilibrium initial state $\rho(0)$. Considering the unperturbed relaxation behavior as given (known), our aim is to draw conclusions about the time evolution of the same initial state when the dynamics is subject to sufficiently weak perturbations.

For example, H_0 may model two isolated subsystems (or a system and its environment), and λV their interaction. If both are prepared in thermal equilibrium states with different temperatures, the perturbation causes a relaxation towards a new thermal equilibrium of the compound system. More generally, already the unperturbed subsystems may exhibit some non-trivial relaxation, which is then modified by the perturbation.

Second, if the considered observable commutes with H_0 (constant of motion), one may ask for the response to a perturbation which breaks the corresponding symmetry. Similarly, the initial state may commute with H_0 (steady state), but not any more with H .

Third, analytical solutions may be available for H_0 but not for H . For instance, H_0 may describe a non-interacting many-body system and V the interactions, or H_0 may be integrable and H non-integrable.

Finally, interesting examples even without a steady long-time limit of the unperturbed system are conceivable and will be covered by our approach.

Focusing on possibly large but finite systems, the Hamiltonian H in (1) exhibits a discrete set of eigenvalues E_n and eigenvectors $|n\rangle$, with n running from one to infinity, or, for instance for a spin model, to some large but finite upper limit. The initial state $\rho(0)$ evolves according to the Schrödinger or von Neumann equation, so that the state at a later time $t > 0$ is given by $\rho(t) = e^{-iHt} \rho(0) e^{iHt}$ ($\hbar = 1$), and the expectation value of an observable (self-adjoint operator) A by

$$\langle A \rangle_{\rho(t)} := \text{Tr}\{\rho(t)A\} = \sum_{m,n} e^{i(E_n - E_m)t} \rho_{mn}(0) A_{nm}, \quad (2)$$

where $\rho_{mn}(t) := \langle m|\rho(t)|n\rangle$ and $A_{nm} := \langle n|A|m\rangle$. Likewise, the corresponding expectation values when the same initial state $\rho(0)$ evolves according to the unperturbed Hamiltonian H_0 with eigenvalues E_n^0 and eigenvectors $|n\rangle_0$ take the form

$$\langle A \rangle_{\rho_0(t)} := \text{Tr}\{\rho_0(t)A\} = \sum_{m,n} e^{i(E_n^0 - E_m^0)t} \rho_{mn}^0(0) A_{nm}^0 \quad (3)$$

with $\rho_{mn}^0(0) := {}_0\langle m|\rho(0)|n\rangle_0$ and $A_{nm}^0 := {}_0\langle n|A|m\rangle_0$.

As usual in this context [10–12], we take for granted that only energies E_n within some sufficiently small energy interval I_E entail non-negligible level populations

$\rho_{nn}(0)$ so that the (locally averaged) mean level spacing ε is approximately constant throughout I_E , and likewise for the unperturbed populations $\rho_{nn}^0(0)$ [5]. This assumption of an approximately constant density of states ε^{-1} for both H_0 and H in particular requires that the perturbation should not become so strong that it modifies the system's thermodynamic properties since the density of states is directly related to (the derivative of) Boltzmann's entropy.

As shown in [4], we thus can replace both $E_n - E_m$ in (2) and $E_n^0 - E_m^0$ in (3) by $(n - m)\varepsilon$ in extremely good approximation. Finally, one can employ the overlaps of the perturbed and unperturbed energy eigenstates,

$$U_{mn} := \langle m|n\rangle_0, \quad (4)$$

to rewrite also the right hand side of (2) in terms of the unperturbed matrix elements $\rho_{mn}^0(0)$ and A_{nm}^0 (see also Sec. VIA). Hence, the comparison between the perturbed and unperturbed relaxation behavior in (2) and (3) essentially boils down to gathering sufficient information about the unitary basis transformation in (4). The simplest idea that immediately comes to mind is to utilize in (1) elementary (Rayleigh-Schrödinger) perturbation theory in order to determine those matrix elements in (4). However, such an approach is limited to exceedingly small λ values in (1) due the extremely large level density ε^{-1} and the concomitant small denominators in such a perturbative treatment. On the one hand, such exceedingly weak perturbations will hardly affect the expectation values in (2) on reasonable time scales at all. For sufficiently strong perturbations, on the other hand, a perturbative expansion of the propagator will generally be limited to uninterestingly small time scales compared to the relevant relaxation time. In other words, some alternative, non-perturbative approach is indispensable.

We thus adopted in [4] the well-established approach [5–7, 17, 18] to temporarily consider an entire statistical ensemble of similar perturbations instead of one particular V in (1) (see also Introduction and Sec. VII for the general conceptual ideas behind such an approach). More precisely speaking, expressing the operator V in the eigenbasis of the unperturbed system, we choose an ensemble of matrices $V_{mn}^0 := {}_0\langle m|V|n\rangle_0$ whose statistics still reflects the essential properties of the “true” perturbation V in (1) as closely as possible. For instance, the V_{mn}^0 may (but need not) exhibit a so-called banded and/or sparse matrix structure. Technically speaking, our main assumptions regarding the admitted random matrix ensembles are that the matrix elements V_{mn}^0 must be statistically independent (apart from $V_{nn}^0 = (V_{nn}^0)^*$) and of zero average (unbiased). Moreover, the second moments (or variances) should only depend – at least within the relevant energy interval I_E and in sufficiently good approximation – on the energy difference $E_m^0 - E_n^0$ of the two levels $|m\rangle_0, |n\rangle_0$ which are coupled via V_{mn}^0 . Recalling that $E_m^0 - E_n^0 \simeq (m - n)\varepsilon$ one might equally well say that the statistical properties (or at least the variances) of the V_{mn}^0 do not depend separately on m

and n , but only on the difference $m - n$. Denoting averages over the ensemble of perturbations by $[\cdots]_V$, those second moments can thus be (approximately) represented as

$$[|V_{mn}^0|^2]_V = \sigma^2(E_m^0 - E_n^0) \quad (5)$$

for some suitable “variance function” or *perturbation profile* $\sigma^2(x)$, which furthermore must satisfy

$$\sigma^2(-x) = \sigma^2(x) \quad (6)$$

due to $V_{nm}^0 = (V_{mn}^0)^*$. Specifically, in cases where V_{mn}^0 exhibits a banded matrix structure (see above), the variances $\sigma^2(x)$ in (5) will approach zero for large energy differences x . Regarding the true perturbation of interest, the key assumption is thus that it exhibits a well-defined perturbation profile in the sense that Eq. (5) holds when replacing the ensemble average $[\cdots]_V$ by a “local” (running) average over close-by energy levels. As a result, $\sigma^2(x)$ is essentially a smooth function by construction. Moreover, the following typicality argument can only be expected to include the true V if the principle mechanism responsible for the dynamical modifications induced by the perturbation is captured by the perturbation profile as the defining property of the considered ensemble (see also the beginning of Sec. VII).

Within this general framework, the main result obtained in Ref. [4] is that, for the overwhelming majority of V ’s in the random matrix ensembles specified above, the perturbed relaxation from (2) will be very well approximated by

$$\langle A \rangle_{\rho(t)} = \langle A \rangle_{\bar{\rho}} + |g(t)|^2 \left\{ \langle A \rangle_{\rho_0(t)} - \langle A \rangle_{\bar{\rho}} \right\} \quad (7)$$

for all λ admitted below Eq. (3). Here $\langle A \rangle_{\rho_0(t)}$ is the unperturbed behavior from (3) and $\bar{\rho}$ is the time-averaged state obtained from $\rho(t)$, i.e., the so-called diagonal ensemble associated with $\rho(0)$ and the perturbed Hamiltonian H from (1) [10–12]. Generically, $\langle A \rangle_{\bar{\rho}}$ is thus expected to coincide with the pertinent thermal value [4, 5, 17, 18]. Finally, the function $g(t)$ in (7) is defined as

$$g(t) := \frac{1}{\pi} \lim_{\eta \downarrow 0} \int dE e^{iEt} \text{Im} G(E - i\eta), \quad (8)$$

where $G(z)$ solves the non-linear integral equation

$$G(z) \left[z - \frac{\lambda^2}{\varepsilon} \int dx G(z - x) \sigma^2(x) \right] = 1. \quad (9)$$

The connection to the perturbed Hamiltonian from (1) is established by observing that the function $G(z)$ encodes the ensemble average of the resolvent or Green’s function $\mathcal{G}(z) := (z - H)^{-1}$ via $G(z - H_0) = [\mathcal{G}(z)]_V$. In particular, the poles of $\mathcal{G}(z)$ correspond to the eigenvalues E_n of H , whereas the matrix elements $\langle m | \mathcal{G}(z) | n \rangle_0$ in the vicinity of these poles are related to the overlaps between the perturbed and unperturbed eigenvectors from (4), see also

Appendix A and the Supplemental Material of Ref. [4] for some additional details.

Overall, these findings (7)–(9) are essentially (apart from some minor technical subtleties) understood to be asymptotically exact for systems with many degrees of freedom, i.e., for large but finite systems there will be some quantitatively unknown subleading order corrections [4]. In particular, the probability to randomly sample a member V of the ensemble which exhibits notable deviations from (7) is exponentially small in the system’s degrees of freedom [4]. More precisely speaking, this probability decreases with the effective number of unperturbed energy levels contributing to any perturbed eigenvector via (4). In principle, the theory may thus equally apply to systems with fewer degrees of freedom provided that they exhibit a sufficiently dense energy spectrum and sufficiently strong mixing of energy levels by the perturbation such that all formal requirements from above are still fulfilled.

Tackling (9) and then (8) by analytical means is the main objective of our present paper.

III. MAIN RESULTS

Before going into the detailed derivations, we briefly summarize the main new findings of our present paper. These consist in relatively simple but expressive representations for the function $g(t)$, which describes how the perturbed dynamics deviates from the unperturbed behavior according to (7).

A first major insight, discussed in detail in Sec. V and derived in Appendix C, is that $g(t)$ solves the non-linear integro-differential equation

$$\dot{g}(t) = -\lambda^2 \int_0^t ds g(t-s) g(s) \tilde{\sigma}^2(s) \quad (10)$$

with the initial condition $g(0) = 1$, where $\dot{g}(t)$ is the derivative of $g(t)$ and

$$\tilde{\sigma}^2(t) := \int \frac{dE}{\varepsilon} e^{iEt} \sigma^2(E) \quad (11)$$

is the Fourier transform of the perturbation profile from (5). Notably, this result resembles common relations for response functions, but is distinctly non-linear. Compared to the indirect representation in terms of Eqs. (8) and (9), the new Eq. (10) exposes the relationship between the system’s response to the perturbation and the perturbation profile $\sigma^2(x)$ much more clearly. Moreover, Eq. (10) considerably simplifies the quantitative evaluation of $g(t)$ for general $\sigma^2(x)$ since it can be solved numerically by standard integration techniques. Not least, it will turn out useful in Sec. VB to assess the asymptotic behavior of $g(t)$ for small and large t .

Our second major insight is an analytical approximation for $g(t)$ that covers practically all cases of physical

relevance and depends on just two parameters of the perturbation V . The first one quantifies its *intrinsic strength*

$$\alpha := \sigma^2(0)/\varepsilon \quad (12)$$

by relating the magnitude $\sigma^2(0)$ of the matrix elements V_{mn}^0 for close-by energy levels [cf. Eq. (5)] to the mean level spacing ε of the unperturbed Hamiltonian [cf. above Eq. (4)]. In view of Eq. (1), the *overall perturbation strength* is thus characterized by $\alpha\lambda^2$. The second parameter assesses the perturbation's energy range or *band width*

$$\Delta_v := \frac{1}{\sigma^2(0)} \int_0^\infty dE \sigma^2(E) . \quad (13)$$

Note that we will also admit cases where the matrix is not banded at all, or where the perturbation profile $\sigma^2(E)$ decays only very slowly with E , so that Δ_v in (13) is infinitely large.

From these two parameters, we can derive the “golden-rule rate” [see the remarks below Eq. (91) for an explanation of the name]

$$\Gamma := 2\pi\lambda^2\alpha \quad (14)$$

as well as the three auxiliary rates

$$\gamma_n := \frac{2\Delta_v}{\pi} \left[1 \pm n\sqrt{1 - \frac{\pi\Gamma}{2\Delta_v}} \right] \quad (15)$$

for $n = -1, 0, 1$. With these definitions, our main result is that $g(t)$ can be excellently approximated for very general perturbation profiles $\sigma^2(x)$ by

$$g(t) = \frac{(\gamma_+ - \frac{\Gamma}{2})e^{-\gamma_-|t|} - \Gamma e^{-\gamma_0|t|} + (\gamma_- - \frac{\Gamma}{2})e^{-\gamma_+|t|}}{2(\gamma_0 - \Gamma)} , \quad (16)$$

where $\gamma_+ \equiv \gamma_1$ and $\gamma_- \equiv \gamma_{-1}$ is understood. This relation will be derived first in Sec. IV as a suitable truncation of the exact result for a special class of perturbation profiles $\sigma^2(x)$. The generalization to largely arbitrary $\sigma^2(x)$ will be achieved in Sec. V by establishing that $g(t)$ is rather insensitive to further details of $\sigma^2(x)$ beyond the parameters α from (12) and Δ_v from (13). Finally, the validity of Eq. (7) in combination with the approximation (16) will also be demonstrated in concrete example systems in Sec. VII.

IV. ANALYTICAL APPROXIMATIONS

For later convenience, we introduce the abbreviation

$$f(x) := \frac{\lambda^2}{\varepsilon} \sigma^2(x) , \quad (17)$$

and – in view of its physical meaning as discussed around (5) – we will often employ the name *perturbation profile*

not only for $\sigma^2(x)$, but also for this function $f(x)$. The integral equation (9) thus takes the form

$$G(z) \left[z - \int dx G(z-x)f(x) \right] = 1 . \quad (18)$$

Our goal in this section is to find (approximate) solutions of (9) by analytical means for the special class of functions $f(x)$ which can be written in the form

$$f(x) = \sum_{n=1}^N \frac{f_n}{1 + (x/a_n)^2} \quad (19)$$

with $f_n \in \mathbb{R}$ and pairwise different $a_n \in \mathbb{R}^+$. The implications of these findings for more general perturbation profiles $f(x)$ will be discussed in Sec. V.

Before going into the actual calculations, we outline the underlying general strategy of our approach: Introducing the complex half-plane

$$\mathbb{C}^- := \{z \in \mathbb{C} \mid \text{Im}(z) < 0\} , \quad (20)$$

our starting point is the assumption that $G(z)$ exhibits the following two properties (at least) for all $z \in \mathbb{C}^-$:

(i) $G(z)$ is analytic. In particular, $G(z)$ thus exists (is well-defined) and is finite (exhibits no singularities).

(ii) $|G(z)| \rightarrow 0$ for $|z| \rightarrow \infty$.

Under these assumptions, and given some perturbation profile $f(x)$ of the form (19), we will then determine approximative solutions of (18), at least for all $z \in \mathbb{C}^-$, and verify that they indeed fulfill the initial assumptions (i) and (ii). Moreover, these approximations can be systematically improved and converge to a (formally) exact solution, which again fulfills (i) and (ii). Accordingly, self-consistent approximate as well as exact solutions will be obtained. Finally, we will also evaluate their Fourier transform $g(t)$ in (8). The question whether these solutions of (18) are unique is quite difficult and addressed in somewhat more detail in Appendix A.

To begin with, we choose an arbitrary but fixed $\eta > 0$ and define

$$\mathbb{C}_\eta^+ := \{z \in \mathbb{C} \mid \text{Im}(z) > -\eta\} , \quad (21)$$

$$\mathbb{C}_\eta^- := \{z \in \mathbb{C} \mid \text{Im}(z) \leq -\eta\} . \quad (22)$$

Since we will later only need asymptotically small η 's in (8), we furthermore can and will assume that $\eta < a_n$ for all n .

Focusing on an arbitrary but fixed $y \in \mathbb{C}_\eta^-$, it follows that $y - z \in \mathbb{C}^-$ for any $z \in \mathbb{C}_\eta^+$. Hence, $F(z) := G(y - z)f(z)$ is a well-defined analytic function on \mathbb{C}_η^+ up to simple poles at $z = ia_n$, which furthermore satisfies $|z^2 F(z)| \rightarrow 0$ for all $z \in \mathbb{C}_\eta^+$ when $|z| \rightarrow \infty$. Under these premises, the integral $\int dx F(x)$ can be readily evaluated by textbook residue techniques, yielding for any given

$y \in \mathbb{C}_\eta^-$ the result

$$\int dx G(y-x)f(x) = \sum_{n=1}^N \tilde{f}_n a_n G(y - ia_n) , \quad (23)$$

$$\tilde{f}_n := \pi f_n . \quad (24)$$

Finally, the integral equation (18) can thus be rewritten in the form

$$G(z) = \frac{1}{z - \sum_{n=1}^N \tilde{f}_n a_n G(z - ia_n)} \quad (25)$$

for all $z \in \mathbb{C}_\eta^-$. Since η in (22) may be arbitrarily small, even arbitrary $z \in \mathbb{C}^-$ are actually admitted in (25).

The remaining task will be to show that a well-defined solution $G(z)$ of (25) exists for all $z \in \mathbb{C}^-$ and that it satisfies the above requirements (i) and (ii). A second key objective will be to determine approximate solutions of this equation (25). The detailed procedure will first be illustrated in the simplest case with $N = 1$ in (19), while for $N > 1$ the generalization of the main results will be provided without repeating all details.

A. Special case $N = 1$

Focusing on $N = 1$ in (19), and adopting the abbreviations

$$a := a_1 , \quad (26)$$

$$\beta := \tilde{f}_1/a , \quad (27)$$

$$H(z) := -ia G(-iaz) , \quad (28)$$

we can rewrite (25) as

$$H(z) = \frac{1}{z + \beta H(z+1)} . \quad (29)$$

In view of Eq. (19) and the definitions (12), (13), and (17), the parameter β can be written as $\beta = \pi^2 \alpha \lambda^2 / 2 \Delta_v$ and thus relates the overall perturbation strength $\alpha \lambda^2$ [see below Eq. (12)] to the band width Δ_v . Hence $\beta \ll 1$ corresponds to weak perturbations, whereas $\beta \gg 1$ amounts to strong perturbations (see also Sec. V).

Analogously to the paragraph below (25), we are now looking for (approximate) solutions of (29) which are, at least for all $z \in \mathbb{C}$ with $\text{Re}(z) > 0$, well-defined (exist), analytic, and satisfy $|H(z)| \rightarrow 0$ for $|z| \rightarrow \infty$. We also remark that, due to (5), (17), and (19), we can and will restrict ourselves to real and positive values of β in (27).

Upon iteration of Eq. (29) one readily obtains

$$H(z) = \frac{1}{z + \beta \frac{1}{z+1+\beta \frac{1}{z+2+\beta \dots}}} , \quad (30)$$

where it is *a priori* understood that the iteration ends after k steps with a term $\beta H(z+k)$ in the last denominator. However, for any given z with $\text{Re}(z) > 0$ and any

$\beta \in \mathbb{R}^+$ it is rigorously shown in Appendix B that the right-hand side of (30) converges towards a well-defined limit as the number of steps tends to infinity. In this sense, the function $H(z)$ in (30) exists (is well-defined) as an infinite continued fraction and is a solution of the original Eq. (29). As already mentioned above Eq. (21), its uniqueness is here tacitly taken for granted and discussed in somewhat more detail in Appendix A. In turn, this yields a formally exact solution $G(z)$ of (18) via (28). Finally, we can conclude that by truncating those continued fraction solutions after a finite number of steps, one obtains approximations which can be systematically improved by including more steps (see also the numerical examples in Fig. 2 below).

In view of the above existence proof of $H(z)$ in (30), it is furthermore quite reasonable to expect that also with respect to other properties of $H(z)$ nothing “dangerous” will happen in any of the nested denominators of the continued fraction expression, at least for any z with $\text{Re}(z) > 0$ and $\beta \in \mathbb{R}^+$. Specifically, it is quite plausible that $H(z)$ will be analytic for any such z . Likewise, upon increasing $|z|$, each dominator grows (in modulus), hence one expects that $H(z)$ approaches zero. In other words, the requirements below (29) are satisfied.

From (30) it follows that $H^*(z) = H(z^*)$, implying for $G(z)$ according to (28) the “symmetry property”

$$G^*(z) = -G(-z^*) . \quad (31)$$

For the usual decomposition of z and $G(z)$ into real and imaginary parts,

$$G(x+iy) = v(x,y) + iw(x,y) , \quad (32)$$

the corresponding symmetries of the real and imaginary parts of $G(z)$ thus take the form

$$v(-x,y) = -v(x,y) , \quad (33)$$

$$w(-x,y) = w(x,y) . \quad (34)$$

Exploiting those symmetries in (8), one readily can conclude, as detailed in Appendix C, that

$$g(t) = \frac{1}{2\pi i} \lim_{\eta \downarrow 0} \int dx G(x - i\eta) e^{ix|t|} \quad (35)$$

and that $g(t)$ is an even and real-valued function of t .

Side remark: Later the integral in (35) will be evaluated by residue methods. Since $G(z)$ is so far only assumed to be analytic for $z \in \mathbb{C}^-$, a finite $\eta > 0$ under the integral is then still needed in principle. In practice, we will actually evaluate the integral mostly for certain approximations of $G(z)$ which will be everywhere analytic up to isolated poles with strictly positive imaginary parts. In this case the limit $\eta \rightarrow 0$ can be performed before the integration. However, in the large β limit (see Sec. IV B) we will also encounter an example where $G(z)$ is indeed non-analytic on almost the entire real axis. In such a case, keeping η finite under the integral is indispensable. Somewhat related issues are also addressed in Appendix A.

Finally, at least for sufficiently small β , a very natural sequence of better and better approximations arises by truncating the continued fraction in (30) later and later. In particular, the first order approximation takes the form

$$H(z) = \frac{1}{z + \beta \frac{1}{z+1}} \quad (36)$$

and likewise for the second order approximation

$$H(z) = \frac{1}{z + \beta \frac{1}{z+1+\beta \frac{1}{z+2}}} , \quad (37)$$

and so on. The corresponding “zeroth order” approximation $H(z) = 1/z$ turns out to be of little use. On the other hand, especially for small $|z|$ also other kinds of approximations, such as $1/[z + \beta]$ or $1/[z + \beta/(z + 1 + \beta/2)]$ etc. could be considered. Generally, we found that the latter approximations are essentially of the same quality as those in (36), (37), and hence we do not further pursue them here.

Next, we rewrite the first order approximation (36) as

$$H(z) = \frac{z+1}{(z+x_1)(z+x_2)} , \quad (38)$$

$$x_{1,2} := \frac{1 \pm \sqrt{1-4\beta}}{2} . \quad (39)$$

This approximative solution is thus analytic (at least) for all $z \in \mathbb{C}$ with $\text{Re}(z) > 0$ (since $\text{Re}(x_{1,2}) > 0$ for any $\beta > 0$), and approaches zero for large $|z|$, i.e., it still satisfies the requirements below (29).

The corresponding approximation for $G(z)$ is recovered upon introducing (38) into (28), yielding

$$G(z) = \frac{z - ia}{(z - ia x_1)(z - ia x_2)} . \quad (40)$$

Finally, inserting (40) into (35) yields by means of standard residue techniques the result

$$g(t) = \frac{x_1 e^{-ax_2|t|} - x_2 e^{-ax_1|t|}}{x_1 - x_2} . \quad (41)$$

While the differentiability properties of (41) are obvious for all $t \neq 0$, the time-point $t = 0$ warrants a closer look. Exploiting (39), one readily confirms that

$$g(0) = 1 , \quad (42)$$

$$\dot{g}(0) = 0 , \quad (43)$$

$$\ddot{g}(0) = -a^2 \beta , \quad (44)$$

and that the third derivative of $g(t)$ does not exist at $t = 0$ (the second derivative is continuous but not differentiable).

Since $\text{Re}(x_{1,2}) > 0$ for any $\beta > 0$ in (39), the right hand side of (41) approaches zero for large t . In the case $\beta < 1/4$, Eq. (39) implies $x_1 > x_2 > 0$, hence the

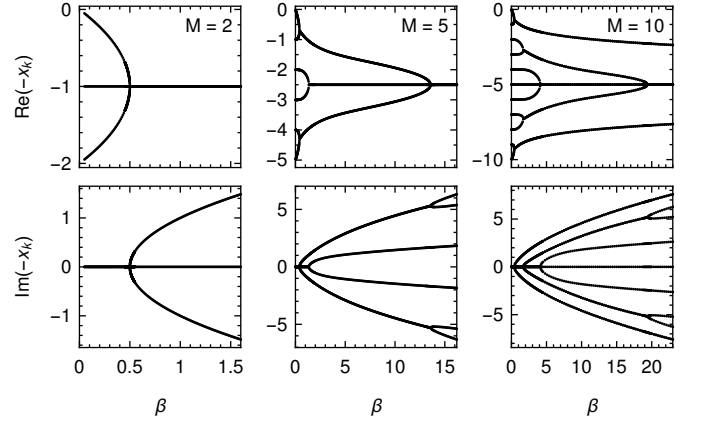


FIG. 1: Real and imaginary parts of the $M+1$ poles versus β for the order- M approximation of $H(z)$ from (30).

large- t asymptotics is dominated by the first summand on the right hand side of (41). For $\beta > 1/4$, the two roots in (39) turn complex, hence (41) amounts to an exponential decay $e^{-a|t|/2}$ times a sinusoidal oscillation. Moreover, for small β one readily recovers the asymptotic approximation

$$g(t) \simeq e^{-\Gamma|t|/2} , \quad (45)$$

where $\Gamma = 2\pi\lambda^2\alpha = 2\pi f_1$ according to (12), (14), (17) and (19). Observing that this approximation violates (43), it follows that the limits $t \rightarrow 0$ and $\beta \rightarrow 0$ do not commute.

Turning to the second order approximation from (37), one can proceed essentially like before. One important observation is that, incidentally, $H(z)$ happens to exhibit a simple pole at $z = -1$, as can be immediately verified by closer inspection of (37). The remaining two poles then readily follow as the solutions of a quadratic equation. Along these lines, one finally arrives at the second order approximation

$$g(t) = \frac{(x_1 - \beta)e^{-ax_2|t|} + (x_2 - \beta)e^{-ax_1|t|} - 2\beta e^{-a|t|}}{2(1-2\beta)} \quad (46)$$

$$x_{1,2} := 1 \pm \sqrt{1-2\beta} , \quad (47)$$

where β is again defined by (27). Likewise, one readily recovers once again the properties in and around Eqs. (42)-(45).

We conclude with some remarks regarding the general structure of the higher-order approximations of the continued-fraction expression (37). Adopting the letter M for the order of the approximation, the first order approximation in (36) thus corresponds to $M = 1$, the second order approximation in (37) to $M = 2$ and so on. Starting with $M = 1$, we found that for small-to-moderate β , both “roots” $x_{1,2}$ in (39) are real and positive, one being close to zero and one close to unity. At $\beta = 1/4$ they turn into a complex conjugated pair with real part $1/2$. The same properties apply to the corresponding poles at $-x_{1,2}$ of $H(z)$ from (38). Analogously,

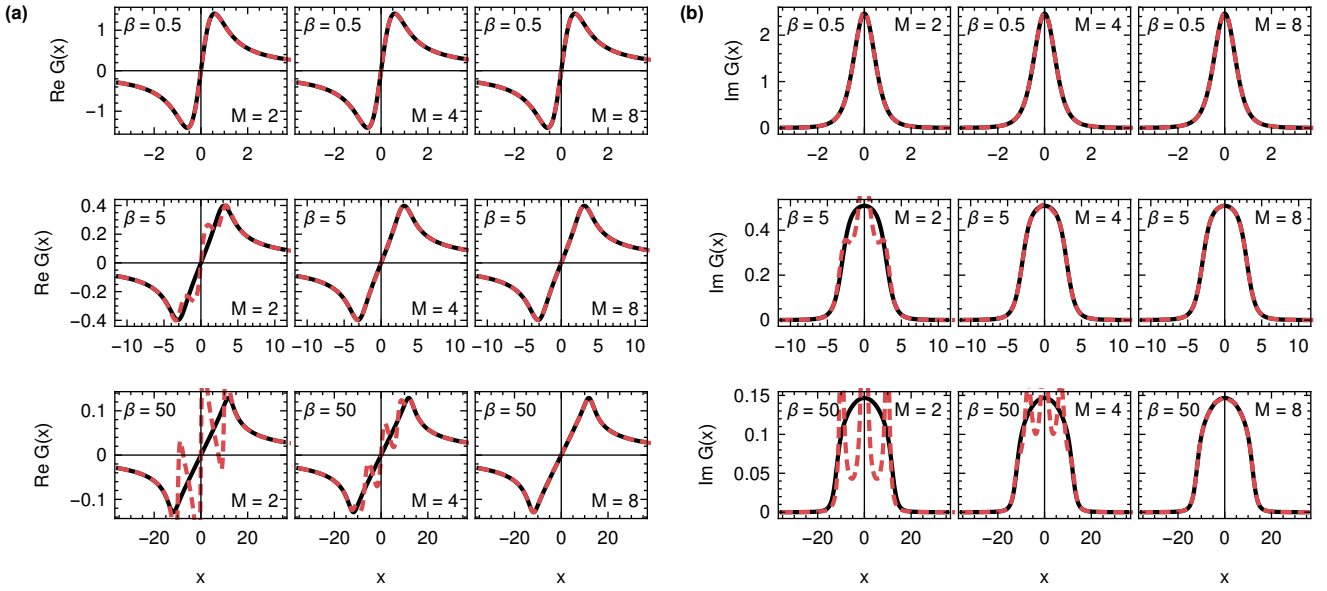


FIG. 2: (a) Real and (b) imaginary parts of the order- M approximations of $G(z)$ for real-valued arguments $z = x$ (dashed, red) together with the corresponding numerically obtained exact solutions (solid, black) of the integral equation (18) with $f(x)$ from (19), $N = 1$, and $a = a_1 = 1$.

for $M = 2$ the two poles at $-x_{1,2}$ are, for small β , real and negative according to (47), one being close to zero and one close to -2 . As β exceeds the value $1/2$, they again turn into a complex conjugated pair with real part -1 . As discussed above (46), there is a third pole which happens to be exactly at -1 for all β . More generally, it thus seems reasonable to expect that the order- M approximation of (30) will exhibit $M + 1$ real- and positive-valued poles close to $0, -1, -2, \dots, -M$ for small β , which turn step by step into complex conjugated pairs upon increasing β . While a more detailed analytical elaboration of this issue seems quite cumbersome, its numerical exploration is straightforward. Fig. 1 depicts the so-obtained numerical findings for several M values, essentially confirming our above expectations. Moreover, for any given M the real part of all poles apparently assumes the same value $-M/2$ for sufficiently large β .

Likewise, with respect to the corresponding order- M approximations for $G(z)$ according to (28), the findings in Fig. 2 quite convincingly demonstrate convergence of the continued-fraction representation for arbitrary β towards the solutions of the original integral equation (18), which we numerically determined as explained in more detail in Ref. [19]. In particular, one expects that all those approximations for $G(z)$ will again satisfy the two requirements below (20) and the symmetry (31), and that the corresponding Fourier transform $g(t)$ from (35) will be a sum of $M + 1$ exponentially decaying functions with the properties (42)-(45) and with decay rates which are given by the $M + 1$ poles from above.

Taking for granted that $G(z)$ satisfies the two requirements below (20) even on the entire lower complex half plane (which is reasonable to expect from the above dis-

cussion of the poles of $G(z)$), it follows that the real and imaginary parts of $G(z)$ are connected via Kramers-Kronig relations, in agreement with how they are seen to behave in Fig. 2.

Finally, the first- and second-order approximations from (41) and (46) are compared with the numerically exact behavior in Fig. 3. More precisely speaking, $|g(t)|^2$ rather than $g(t)$ itself is plotted since it is this quantity which actually matters in (7). Clearly, the agreement is practically perfect for the second-order approximation, apart from very large β -values and times considerably larger than the relaxation time of the exact $|g(t)|^2$. The latter shortcoming could be readily remedied by switching to the large- β approximation (thin dashed lines, see Eq. (55) below) when $a^2\beta$ exceeds some critical value, e.g., $a^2\beta > 10$. Moreover, also the higher-order approximations would exhibit even much smaller such deviations, hence they are not shown.

The very good performance of the second order approximation for $g(t)$ is remarkable for two reasons. First, in its original derivation we assumed that β is small. Second, the corresponding $M = 2$ approximations for $G(x)$ in Fig. 2 indeed show much more pronounced deviations for larger values of β . We observe that these deviations are most striking in the region around $x = 0$, whereas the tails are generally reproduced well already for small M and large β . Since $g(t)$ is essentially the Fourier transform of $\text{Im } G(x)$ [see Eq. (35)], the short-time behavior is mainly determined by those tails and the deviations for small x become effective only later when the exact $|g(t)|^2$ has basically relaxed to zero for all practical purposes (cf. Fig. 3).

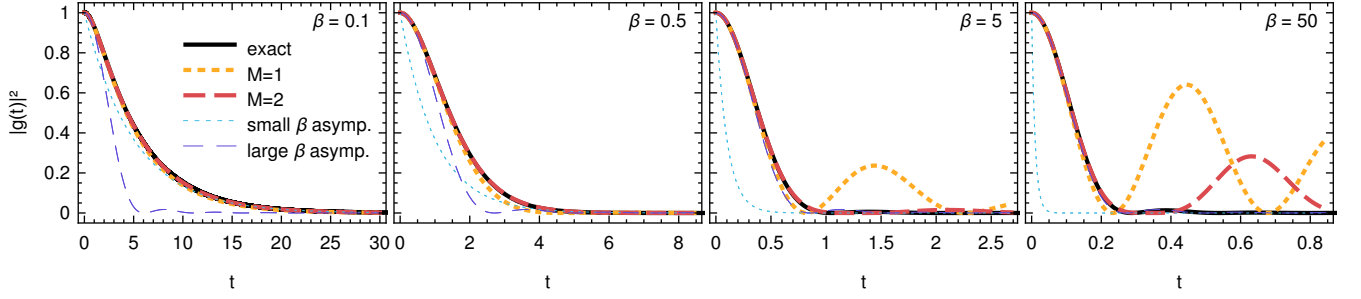


FIG. 3: Analytic approximations of $|g(t)|^2$ versus numerically exact results for the perturbation profile (19) with $N = 1$, $a = a_1 = 1$, and various values of β (note the different scales of the t -axis). Bold solid lines: Numerically exact solutions of (8) and (9). Bold dotted lines: First order approximations from (41). Bold dashed lines: Second order approximations from (46). Thin dotted lines: Small β asymptotics from (45). Thin dashed lines: Large β asymptotics from (55).

B. Large β asymptotics for $N = 1$

With the definition

$$I(z) := \sqrt{\beta} H(\sqrt{\beta} z) \quad (48)$$

we can rewrite (29) as

$$I(z) = \frac{1}{z + I(z + 1/\sqrt{\beta})}. \quad (49)$$

For asymptotically large β we thus can conclude that

$$I(z)[I(z) + z] - 1 = 0 \quad (50)$$

and therefore

$$I(z) = \frac{-z \pm \sqrt{4 + z^2}}{2}. \quad (51)$$

Returning to $G(z)$ via (48) and (28) yields

$$G(z) = \frac{2}{\gamma^2} \left[z \pm i\sqrt{\gamma^2 - z^2} \right], \quad (52)$$

$$\gamma := 2a\sqrt{\beta}. \quad (53)$$

As usual, the complex square root is defined here as $\sqrt{z} := \exp\{\ln(z)/2\}$, where $\ln(z) := \ln(|z|) + i\arg(z)$, and where $\arg(z)$ is the principal value argument of the complex number z . Hence, the right hand side of (52) is, for either choice of the sign, analytic apart from cuts on $(1, \infty)$ and $(-\infty, -1)$, i.e., the second requirement below (20) is fulfilled. However, the first requirement below (20), $|G(z)| \rightarrow 0$ for $z \in \mathbb{C}^-$ with $|z| \rightarrow \infty$, is only fulfilled when choosing the plus sign in (52), resulting in

$$G(z) = \frac{2}{\gamma^2} \left[z + i\sqrt{\gamma^2 - z^2} \right]. \quad (54)$$

Finally, also the symmetry property (31) is again fulfilled, as can be inferred from (54) by exploiting that $\sqrt{z^*} = (\sqrt{z})^*$.

The corresponding function $g(t)$ is most conveniently obtained by introducing (54) directly into the definition (8), yielding

$$g(t) = 2J_1(\gamma t)/\gamma t, \quad (55)$$

where $J_1(x)$ is the Bessel function of the first kind of order 1. Remarkably, one thus recovers once again exactly the same properties as in (42)-(44). But in contrast to the remark below (44), now also all higher derivatives of $g(t)$ exist at $t = 0$. Finally, the large- t asymptotics of (55) amounts to a decay proportional to $|t|^{-3/2}$ times a sinusoidal oscillation, again somewhat similar to the findings for large β above (45), albeit the decay is now given by a power law rather than an exponential. In fact, as will be demonstrated in more detail in Sec. VB [see the discussion below Eq. (90)], the limits $\beta \rightarrow \infty$ and $t \rightarrow \infty$ do not commute, so the present $|t|^{-3/2}$ asymptotics will ultimately cross over to an exponential decay for any preset (finite) value of β .

One possibility to determine the first order correction to the above asymptotics (54) would be to rewrite (49) as

$$I(z)[I(z) + d(z) + z] - 1 = 0, \quad (56)$$

$$d(z) := I(z + 1/\sqrt{\beta}) - I(z), \quad (57)$$

and then to approximate the small difference on the right hand side of (57) by means of the previous approximation from (54). But since the integral in (8) is then likely to only be tractable by numerical means, we do not further pursue this issue.

C. General N

Next we briefly sketch the generalizations of the so far employed considerations when going over from $N = 1$ to arbitrary N in (19): In terms of the same auxiliary function $H(z)$ as in (28) one readily obtains from (25) as

a generalization of (30) the continued fraction form

$$H(z) = \frac{1}{z + \sum_{n=1}^N \beta_n H(z + \tilde{a}_n)} \quad (58)$$

$$= \frac{1}{z + \sum_{n=1}^N \beta_n \frac{1}{z + \tilde{a}_n + \sum_{m=1}^N \beta_m \frac{1}{z + \tilde{a}_n + \tilde{a}_m + \dots}}} \quad (59)$$

$$\tilde{a}_n := a_n/a, \quad (60)$$

$$\beta_n := \tilde{f}_n a_n / a^2. \quad (61)$$

Here, the quantity a can still be chosen arbitrarily. For instance, the previously considered special case with $N = 1$ is readily recovered by choosing $a = a_1$, implying $\tilde{a}_1 = 1$ and $\beta_1 = \tilde{f}_1/a$ (cf. (27)). Another natural choice is $a = 1$, implying $\tilde{a}_n = a_n$ and $\beta_n = \tilde{f}_n a_n$. For the rest, it is reasonable to expect that conclusions analogous to those below (30) will also apply to the function $H(z)$ in (59). Most importantly, Eqs. (59) and (28) again imply the same symmetry property of $G(z)$ as in (31) and hence the same relation for $g(t)$ as in (35).

Focusing on sufficiently small β_n , the generalization of the previous first-order approximation (36) now takes the form

$$H(z) = \frac{1}{z + \sum_{n=1}^N \beta_n \frac{1}{z + \tilde{a}_n}} = \frac{1}{-h(-z)} \quad (62)$$

$$h(z) := z + \sum_{n=1}^N \frac{\beta_n}{z - \tilde{a}_n} \quad (63)$$

By means of a graphical sketch of the function $h(x)$ for $x \in \mathbb{R}$, one readily sees that the equation $h(x) = 0$ generically exhibits $N + 1$ solutions, which are all real-valued and positive, and which we denote by x_k with $k = 1, \dots, N + 1$, i.e.,

$$h(x_k) = 0 \text{ with } x_k \in \mathbb{R}^+ \text{ and } k = 1, \dots, N + 1. \quad (64)$$

Furthermore, for sufficiently small β_n , one finds that one solution of $h(x) = 0$ is close to zero, and that all further solutions are close to one of the \tilde{a}_n 's. Without loss of generality, we may thus choose the labels so that $x_{N+1} \simeq 0$ and $x_n \simeq \tilde{a}_n$ for $n = 1, \dots, N$. Accordingly, it is natural to make the ansatz $x_n = -\tilde{a}_n + \delta_n + \delta'_n + \dots$ and $x_{N+1} = \delta_{N+1} + \delta'_{N+1} + \dots$, where the δ_k (for $k = 1, \dots, N + 1$) are of first order in the small parameters β_n , the δ'_k of second order, and the terms “+...” of higher order. Introducing this ansatz into (63), (64) and solving the equations order by order then yields the result (up to first order in the β_n)

$$x_n \simeq \tilde{a}_n - \frac{\beta_n}{\tilde{a}_n} \text{ for } n = 1, \dots, N, \quad (65)$$

and (up to second order in the β_n)

$$x_{N+1} \simeq \left(\sum_{n=1}^N \frac{\beta_n}{\tilde{a}_n} \right) \left(1 + \sum_{n=1}^N \frac{\beta_n}{\tilde{a}_n^2} \right). \quad (66)$$

Rewriting (62) as

$$H(z) = q(z)/p(z), \quad (67)$$

$$q(z) := \prod_{n=1}^N (z + \tilde{a}_n), \quad (68)$$

$$p(z) := z q(z) + \sum_{n=1}^N \beta_n \prod_{m=1, m \neq n}^N (z + \tilde{a}_m), \quad (69)$$

one readily concludes that $p(z)$ is a polynomial of the form $z^{N+1} + \dots$, whose zeroes must coincide with the $-x_k$'s from above, i.e.,

$$p(z) = \prod_{k=1}^{N+1} (z + x_k) \quad (70)$$

Together with (28), (67), and (68) we thus arrive at the approximation

$$G(z) = \frac{\prod_{n=1}^N (z - i\tilde{a}_n)}{\prod_{k=1}^{N+1} (z - iax_k)}. \quad (71)$$

Finally, the integral in (35) can again be evaluated by standard residue methods, resulting in

$$g(t) = \sum_{k=1}^{N+1} A_k e^{-ax_k|t|}, \quad (72)$$

$$A_k := \frac{\prod_{n=1}^N (\tilde{a}_n - x_k)}{\prod_{j=1, j \neq k}^{N+1} (x_j - x_k)}. \quad (73)$$

Exploiting (65) and (66) yields for the amplitudes A_k in (73) the approximations

$$A_n \simeq -\frac{\beta_n}{\tilde{a}_n^2} \text{ for } n = 1, \dots, N, \quad (74)$$

$$A_{N+1} \simeq 1 + \sum_{n=1}^N \frac{\beta_n}{\tilde{a}_n^2}. \quad (75)$$

By means of those approximations, one again recovers the properties in and around Eqs. (42)-(45) [see also below Eq. (47)], except that Γ and β now take the form

$$\Gamma = 2\pi \lambda^2 \frac{\sigma^2(0)}{\varepsilon} = 2\pi \sum_{n=1}^N f_n, \quad (76)$$

$$\beta := \sum_{n=1}^N \beta_n. \quad (77)$$

Turning finally to the case of asymptotically large β_n , we employ the same auxiliary function $I(z)$ as in (48) with β from (77). Introducing these quantities into (58) yields as a generalization of (49) the result

$$I(z) = \frac{1}{z + \sum_{n=1}^N \frac{\beta_n}{\beta} I(z + \tilde{a}_n/\sqrt{\beta})}. \quad (78)$$

For asymptotically large β , all further conclusions remain exactly the same as in (50)-(55).

V. UNIVERSALITY PROPERTIES OF $g(t)$

Despite the large variability of admissible perturbations with the properties described in and around Eqs. (5) and (6), the function $g(t)$, which governs the perturbed relaxation in (2) and (7), will turn out to be surprisingly universal. The aim of this section is to track down the origins of this universality. For this purpose, we will explore how $g(t)$ varies with the perturbation strength and with time. In both cases, the limiting expressions for small and large values will be found to be determined by the overall strength $\alpha\lambda^2$ [see below Eq. (12)] and the band width Δ_v [see Eq. (13)] of the perturbation alone. In addition, we will inspect several other shapes of the perturbation profile function $\sigma^2(x)$ and the stability of $g(t)$ against those variations. Exploiting the universality of $g(t)$, we will finally be able to condense the perturbation dependence of the prediction (7) for the perturbed relaxation to just these two parameters, culminating in the main result (16).

A. Asymptotics and crossover with respect to the coupling strength λ

For our special class of functions $f(x)$ from (19) one readily finds with (12), (13), and (17) the relations

$$\alpha\lambda^2 = \sum_{n=1}^N f_n, \quad (79)$$

$$\Delta_v = \frac{\pi}{2} \frac{\sum_{n=1}^N a_n f_n}{\sum_{n=1}^N f_n}. \quad (80)$$

By exploiting (61) and (77) it follows that

$$\beta = 2\lambda^2\alpha\Delta_v/a^2 \quad (81)$$

and with (44) that

$$\ddot{g}(0) = -2\lambda^2\alpha\Delta_v. \quad (82)$$

Together with (76) we thus recover the definition $\Gamma := 2\pi\lambda^2\alpha$ from (14), and with (53) we find that

$$\gamma = \lambda\sqrt{8\alpha\Delta_v}. \quad (83)$$

For fixed α and Δ_v , it follows from (81) that the regimes of small and large β are equivalent to small and large coupling strengths λ in (1), respectively [see also the comment below Eq. (29)]. Hence (45) now applies for small λ and is, according to (14), entirely determined by the parameter α , independently of any further details of the function $f(x)$ in (19). Likewise, (55) applies for large λ and solely depends on the parameters α and Δ_v via (83).

As expected in view of (45) and (55), and elaborated in somewhat more detail in Ref. [4], the “crossover” between the two asymptotic regimes is roughly determined

by the condition $\Gamma = \gamma$. According to (14) and (83), the corresponding crossover coupling strength is thus given by

$$\lambda_c := \sqrt{2\Delta_v/\pi^2\alpha}, \quad (84)$$

i.e., the asymptotics from (45) and (55) are expected to apply for $\lambda \ll \lambda_c$ and $\lambda \gg \lambda_c$, respectively.

As shown in more detail in Ref. [19], the above discussed asymptotics for large and small λ in fact apply not only for functions $f(x)$ in (17) of the form (19), but even for largely arbitrary perturbation profiles $f(x)$ and thus $\sigma^2(x)$ in (17), and likewise for the crossover condition $\Gamma \approx \gamma$ implying (84).

Furthermore, for perturbations which are not banded or only very weakly banded, so that the band width in (13) is infinitely large (see discussion below (13)), the approximation (45) is in view of (84) expected to actually apply for all values of the coupling strength λ [20] (provided they are still compatible with the overall restrictions for λ discussed in Sec. II).

The above predicted structural stability of the function $g(t)$ for asymptotically small and large λ and of the crossover value from (84) are also illustrated in Fig. 5 below, where we compare numerical solutions of $g(t)$ for various perturbation profiles $\sigma^2(x)$ and coupling strengths λ .

B. Asymptotics and crossover with respect to time

Interestingly, an analogous crossover between (45) and (55) can also be observed in the time domain for a fixed value of λ . Our starting point is the non-linear integro-differential equation (10), which can be obtained – as detailed in Appendix C – via Fourier transformation of (18). Exploiting (17), it reads

$$\dot{g}(t) = - \int_0^t ds g(t-s) g(s) \tilde{f}(s), \quad (85)$$

$$\tilde{f}(t) := \int dx e^{ixt} f(x) \quad (86)$$

$$g(0) = 1, \quad (87)$$

see also (42). From this equation (85), it is straightforward to deduce a relation between the coefficients of a Taylor expansion of $g(t)$ around $t = 0$ and the moments

$$F_k := \int dx x^k f(x) \quad (88)$$

of the perturbation profile (if they exist, see also below (44)). For our present purpose, an even simpler argument is sufficient: For small t , the integrand $g(t-s)g(s)\tilde{f}(s)$ in (10) can be approximated in leading order by $[g(0)]^2\tilde{f}(0)$, yielding with (87)

$$g(t) \simeq 1 - \frac{1}{2}\tilde{f}(0)t^2 = 1 - \lambda^2\alpha\Delta_v t^2, \quad (89)$$

where we exploited (12), (13), (17), and (86) in the last equality, and where we tacitly assumed that $\tilde{f}(0)$ and

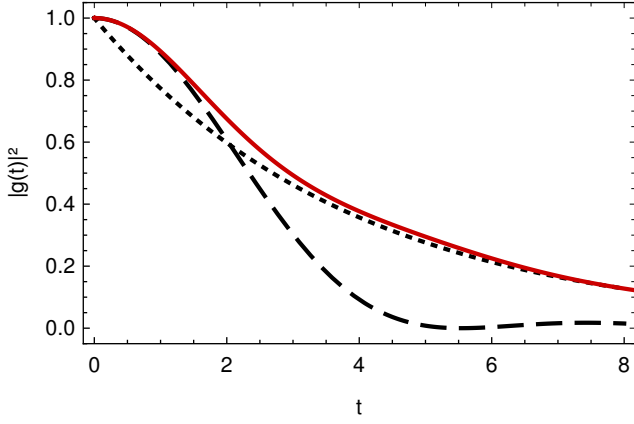


FIG. 4: Numerical solution for $|g(t)|^2$ (solid) for the step perturbation profile $f(x) = 0.04 \Theta(1.5^2 - x^2)$ with band width $\Delta_v = 1.5$ compared to the asymptotic decay characteristics for weak [dotted, Eq. (45)] and strong [dashed, Eq. (55)] perturbations. This illustrates the transition in the time domain from the Bessel-type behavior for $t \ll t_c$ to the exponential behavior for $t \gg t_c$ with $t_c \approx \pi/\Delta_v \approx 2.1$.

hence the band width Δ_v are finite. In particular, this is in agreement with our previous findings (42), (43), and (82) for the special class of functions from (19). Remarkably, even the approximation for large λ from (55) can be shown to exhibit the same asymptotic behavior for small t as in (89).

On the other hand, in the so far excluded case that $\tilde{f}(0)$ and hence the band width Δ_v are infinite, one finds that $\tilde{f}(t)$ in (86) generically develops a δ -peak at $t = 0$. By means of analogous calculations as before one then recovers from (10) the same small- t asymptotics as in (45), i.e., $g(t) \simeq 1 - \Gamma |t|/2$ with Γ from (14). Similarly as below (45), we thus arrive at the important conclusion that *the limits $t \rightarrow 0$ and $\Delta_v \rightarrow \infty$ do not commute*.

The asymptotic behavior of $g(t)$ for large t can be extracted from (10) by means of the ansatz $g(t) = e^{-rt}$. Substituting into (10), we find that

$$r = \int_0^t ds \tilde{f}(s) \rightarrow \pi f(0) = \pi \alpha \lambda^2 \quad (t \rightarrow \infty). \quad (90)$$

For large t , we thus conclude that $g(t) \sim e^{-\pi \alpha \lambda^2 t}$ coincides with the limiting expression (45) for small λ or large Δ_v with Γ given in (14). In contrast, the asymptotic behavior (55) for large λ exhibits a power-law decay $\sim t^{-3/2}$ as $t \rightarrow \infty$. Similarly as before, we thus find that the limits $t \rightarrow \infty$ and $\lambda \rightarrow \infty$ do not commute either. But since too large λ values are physically unrealistic, the actual main conclusion is that the asymptotics (55) must always become invalid for sufficiently large t .

Similarly as in (84), an estimate for the “crossover” time at which the exponential regime sets in can be found by equating (89) with the asymptotic form $e^{-\pi \alpha \lambda^2 t} \approx 1 - \pi \alpha \lambda^2 t$, yielding

$$t_c \approx \pi/\Delta_v, \quad (91)$$

independent of λ and α [6].

Altogether, we thus can conclude that the small- t asymptotics of $g(t)$ is (for any finite band width Δ_v) described by (55), while (45) captures the large- t asymptotics, and that the crossover time scale is solely determined (to leading order) by the inverse band width according to (91). In particular, the two asymptotic approximations in (45) and (55) actually do not only apply to small and large λ , but also to large and small t , respectively.

At this point it is noteworthy that Eq. (7) entails, incidentally, a non-perturbative justification of Fermi’s golden rule [21] in the present many-body setting [22]. More precisely, our universal long-time asymptotics with $|g(t)|^2 \sim e^{-\Gamma t}$ and $\Gamma = 2\pi \lambda^2 \sigma^2(0) \varepsilon^{-1}$ [see Eqs. (12) and (90)] comprises as a special case the “standard” golden rule for the transition probability from one unperturbed eigenstate $|n_i\rangle_0$ to another (sufficiently close) one $|n_f\rangle_0$ by choosing $\rho(0) = |n_i\rangle_0 \langle n_i|$ and $A = |n_f\rangle_0 \langle n_f|$. Indeed, the rate Γ is then proportional to the (ensemble-averaged) squared perturbation matrix element $[\lambda^2 |V_{n_i n_f}|^2]_V \simeq \lambda^2 \sigma^2(0)$ and the density of states ε^{-1} as predicted by the golden rule. Our present asymptotic analysis thus suggests that the relaxation characteristics of perturbed many-body systems can be described by Fermi’s golden rule for sufficiently weak perturbations at sufficiently late times. Crucially, we also quantify how the relaxation behavior changes beyond this regime when $|g(t)|^2$ deviates from the exponential form [see also, in particular, Eq. (16) and its justification in Sec. V C].

The transition in the time domain predicted around Eq. (91) is illustrated in Fig. 4 for a step profile $f(x) = 0.04 \Theta(1.5^2 - x^2)$ [cf. Eq. (17)], where $\Theta(x)$ denotes the Heaviside step function. The step profile is chosen because the transition is very sharp here compared to “more regular” shapes [19].

We also remark that a similar transition was observed in Ref. [6] for the response of a small system coupled to a bath, modeled by a related random-matrix setup where the perturbation profile (5) was assumed to be given by a step function, too (see also Sec. VIB for a more detailed comparison of our work and Ref. [6]). More precisely speaking, based on a small- t expansion and numerical evidence, the authors of Ref. [6] predicted a Gaussian decay for $t \ll \Delta_v^{-1}$, whose asymptotic behavior is consistent with (89), and an exponential decay with rate (90) for $t \gg \Delta_v^{-1}$.

Combining the observations from Secs. V A and V B, we expect that the decay characteristic on the relevant time scales where $g(t)$ notably deviates from zero is predominantly exponential for $\lambda \lesssim \lambda_c$ and predominantly Bessel-like for $\lambda \gtrsim \lambda_c$ with λ_c from (84). Since the relaxation time scale associated with λ_c (obtained by substituting λ_c into Γ^{-1} from (14) or γ^{-1} from (83)) is $t_c/4$, the transition in the time domain will usually only be observable in the weak-perturbation regime with $\lambda \lesssim \lambda_c$.

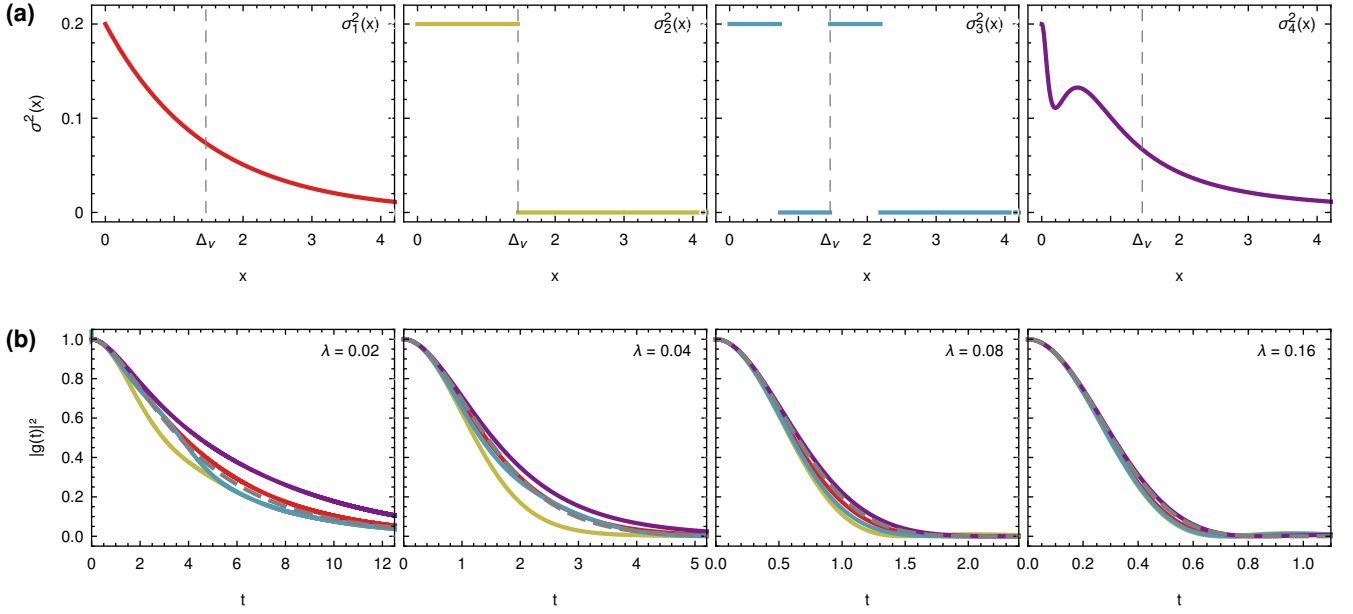


FIG. 5: (a) Four different perturbation profiles $\sigma^2(x)$, each with $\sigma^2(0) = 0.2$ and $\Delta_v = 1.5$: exponential profile $\sigma_1^2(x) = \sigma^2(0) e^{-|x|/\Delta_v}$ (red), step profile $\sigma_2^2(x) = \sigma^2(0) \Theta(\Delta_v^2 - x^2)$ (yellow), two-step profile $\sigma_3^2(x) = \sigma^2(0) \mathbb{1}_{[0, \Delta_v/2] \cup [\Delta_v, 3\Delta_v/2]}(|x|)$ with $\mathbb{1}_S(x)$ denoting the indicator function of the set S (blue), sum of four Breit-Wigner functions (5), $\sigma_4^2(x)$, with $N = 4$, $a_1 = 2a_2 = 4a_3 = 8a_4 = 0.93$, $2f_1/3 = -f_2 = -2f_3 = f_4 = \sigma^2(0) = 0.2$ (purple). (b) Corresponding numerically exact solutions $|g(t)|^2$ with $\varepsilon = 0.002$ (hence $\alpha = 100$) for various coupling strengths λ as indicated in the top-right corner of each panel (note the different scales of the t -axis). Additionally, the gray dashed line in every panel (sometimes hardly visible) represents the analytical approximation (16).

C. Refined prediction of perturbed relaxation

Next we turn to the question of how general (or special) our analytically considered class of functions $\sigma^2(x)$ of the form (17), (19) actually is. To begin with we recall that the Fourier transform $\tilde{h}(k) := \int dx e^{-ikx} h(x)$ of the function $h(x) := [1 + (x/a)^2]^{-1}$ is $\tilde{h}(k) = a\pi e^{-a|k|}$. Accordingly, the Fourier transform of $f(x)$ from (19) is of the form $\tilde{f}(k) = \sum_{n=1}^N b_n e^{-a_n|k|}$ with largely general $a_n \in \mathbb{R}^+$ and $b_n := \pi a_n f_n \in \mathbb{R}$. In turn, from the method of Laplace transformations one can conclude that a very large class of functions $\tilde{f}(k)$ can be written – at least in very good approximation – as sums of exponentially decaying terms. In conclusion, the functions $f(x)$ of the form (19) are actually expected to cover a very large class of different functions $\sigma^2(x)$ in (17). Since $\sigma^2(x)$ is a smooth function by construction as mentioned below Eq. (6), it may even be expected that (19) essentially covers all cases of notable interest.

In particular, the symmetry (31) is thus predicted to be fulfilled very generally, and $g(t)$ in (8) to be even and real-valued (see below (35)).

Since, as pointed out above, all those perturbation profiles $\sigma^2(x)$ with identical parameters α and Δ_v entail very similar functions $g(t)$ for sufficiently small and large λ (and likewise for sufficiently small and large t), it is interesting to explore in more detail how much those functions $g(t)$ will differ for intermediate values of λ (or of

t). While we did not succeed to arrive at any interesting analytical insights along these lines, the numerical results presented in Fig. 5 very convincingly show that the functions $g(t)$ actually depend very little on any further details of $\sigma^2(x)$, once the values of λ , α , and Δ_v are fixed.

On the other hand, we found in Sec. IV B that the second-order approximation (46) reproduces the exact behavior remarkably well for perturbation profiles $f(x)$ of the form (19) with $N = 1$. Rewriting this approximation (46) in terms of the two parameters α and Δ_v according to (79)-(81) thus yields as a very general prediction for the function $g(t)$ the approximation (16) as stated in Sec. III. For comparison, this approximation is also displayed in Fig. 5 as dashed gray lines. Furthermore, even better agreement with the results for different perturbation profiles could be achieved by introducing “renormalized” parameters α and Δ_v to approximate them by the Breit-Wigner shape (19).

Altogether, Eqs. (7) and (16) thus amount to a fully analytical prediction for the perturbed relaxation behavior in terms of only two very basic characteristics of the perturbation, namely the (intrinsic) perturbation strength from (12) and the band width (or perturbation range) from (13). This is the main result of our present paper.

VI. COMPARISON WITH RELATED PREVIOUS WORKS

The question of how the observable relaxation behavior of an unperturbed many-body system is modified in response to a weak perturbation is very natural. Accordingly, various aspects of this general question have been addressed in a considerable number of previous works. Before discussing in somewhat more detail those which are particularly close to our present paper, we exemplify that even rather strong approximations may still lead to quite decent results in this context.

A. Simple approximation

In a first step, we employ the basis transformation (4) to rewrite the right hand side of (2) in terms of the unperturbed matrix elements of $\rho(0)$ and A , resulting after a couple of elementary manipulations in

$$\langle A \rangle_{\rho(t)} = \sum_{k,l,m,n} e^{i(E_n^0 - E_m^0)t} \rho_{kl}^0(0) A_{nm}^0 S_{km}^*(t) S_{ln}(t), \quad (92)$$

$$S_{km}(t) := \sum_{\mu} e^{i(E_{\mu} - E_m^0)t} U_{\mu k}^* U_{\mu m}. \quad (93)$$

In view of the orthonormality relation $\sum_{\mu} U_{\mu k}^* U_{\mu m} = \delta_{km}$, it seems reasonable to expect that, within a very crude approximation, the sum on the right hand side of (93) is negligibly small unless $k = m$. In turn, for $k = m$ the factors $|U_{\mu m}|^2$ can be reasonably well approximated by their ensemble-averaged values $[|U_{\mu m}|^2]_V$. The main argument is that the sum consist of so many terms of similar character that – much like in the common central limit theorem – a kind of “self-averaging” effect can be expected. Due to analogous arguments as above (5), this average can furthermore be written in the form

$$[|U_{\mu m}|^2]_V = u(E_{\mu}^0 - E_m^0) \quad (94)$$

for some suitable function $u(E)$ (see also (A5)), and the differences $E_{\mu} - E_m^0$ in (93) and $E_{\mu}^0 - E_m^0$ in (94) can be roughly approximated by $(\mu - m)\varepsilon$. Altogether we thus arrive at

$$S_{km}(t) \simeq \delta_{km} \tilde{g}(t), \quad (95)$$

$$\tilde{g}(t) := \sum_n e^{in\varepsilon t} u(n\varepsilon). \quad (96)$$

Taking into account (92) and (3), we thus can conclude that

$$\langle A \rangle_{\rho(t)} \simeq |\tilde{g}(t)|^2 \langle A \rangle_{\rho_0(t)}. \quad (97)$$

Anticipating that $\tilde{g}(t)$ will turn out to coincide with $g(t)$ (see also Eqs. (A5) and (A8)), the similarity of (97) and (7) is remarkable. If the long-time limit $\langle A \rangle_{\bar{\rho}}$ in (7) happens to vanish, the two relations are even identical.

The main shortcoming of our above “quick and dirty” derivation is that (97) is clearly wrong if A is the identity operator. More generally, (7) exhibits a wrong transformation behavior when adding a constant to A . A more detailed inspection [4, 18] reveals two main reasons for this deficiency: Though the terms in (93) with $k \neq m$ are indeed very small, there are so many of them which contribute to (92) that they cannot be neglected. Similarly, there are very weak but very numerous “correlations” between the summands in the two S -factors in (92), which also sum up to a non-negligible correction. Yet another shortcoming is the fact that all those arguments appear reasonable at most in cases where the basis transformation U_{mn} from (4) behaves in a “typical” manner, which cannot be specified more precisely. In particular, the likelihood to encounter an “exception” remains unknown.

Apart from those issues, the main point of the above exercise is to demonstrate that at least the basic structure of the correct result from (7) is remarkably robust against quite crude approximations in its derivation.

B. Connections to pertinent previous works

The overall setting of our approach, involving a reference Hamiltonian H_0 perturbed by an ensemble of random matrices, is similar to Deutsch’s seminal paper [5]. In this early work, the considered perturbations are taken from the Gaussian orthogonal ensemble (GOE) and thus do not emulate the sparsity and bandedness properties found in many physical examples, but the pertinent modifications are subordinate with respect to the questions studied in [5], see also [4, 17, 19]. Namely, Ref. [5] establishes that the absence of thermalization in many-body quantum systems is fragile in the sense that small perturbations will typically lead to thermal equilibrium phenomenology in the long-time limit. To do so, Deutsch devised a computational scheme [23] to approximately calculate ensemble averages for products of eigenvector overlaps (4) between the unperturbed and perturbed systems. In particular, from the so-obtained results for the second moments in (94) one can infer that the function $\tilde{g}(t)$ in (95) indeed agrees with our previous $g(t)$ from (8) for the considered special case that the perturbation matrices are sampled from a GOE. It is therefore no surprise that such eigenvector overlap moments are actually also at the heart of the derivations in Ref. [4] (see also Eqs. (A5) and (A8)), even though different methods were used there for their evaluation. Also note that the focus of our present work (as well as its predecessors [4, 19]) is on the dynamical relaxation process rather than the equilibrium (long-time average) properties.

Using Deutsch’s random matrix model, and extending his approximative methodology, Nation and Porras [7] found a result akin to Eq. (7) for the time evolution of expectation values with the special choice $g(t) = e^{-\Gamma t/2}$. Since the perturbations were again sampled from a GOE, whose band width in (13) is infinite, this is in agree-

ment with the special case discussed below (83). Technically speaking, their approximation includes some of the omitted small terms discussed below (97), while others are still missing as a consequence of the fact that some basic orthonormality properties of the unitary matrix U_{mn} are not properly accounted for (see equation (48) in [18]). As a consequence, considerable restrictions with respect to the class of admitted observables A had to be made in [7], requiring a special type of sparsity where only a few off-diagonals of the matrix A_{mn}^0 [see below Eq. (3)] may exhibit nonvanishing entries. Furthermore, the concentration-of-measure property, crucial for turning ensemble averages into predictions about the overwhelming majority of individual members of the considered perturbation ensemble (see above (7)), was merely postulated rather than proved in Ref. [7].

By means of yet another approach, based on a Lippman-Schwinger-type equation, Ithier and Ascroft evaluated special cases of the eigenvector overlap moments in Deutsch's random matrix ensemble up to fourth order [24], which are needed in the last two factors in (92) when evaluating the ensemble average of that equation.

The investigation of significantly more general random matrix ensembles of the form (1), covering, among others, perturbations exhibiting a sparse and/or banded structure, has a long-standing history as well, see, e.g., Refs. [25–36] and references therein. Particularly noteworthy in our present context is the work [35] by Fyodorov et al., who studied the statistical properties of banded and sparse random matrix ensembles closely related to the perturbation ensembles in [4, 19] and the present work. Notably, the integral equation (9) is equivalent to an integral equation which was obtained in a similar but different context in Ref. [35]. Namely, by means of the definition $g_\kappa(z) := i[G(z)^{-1} - z]$ one readily recovers from our Eq. (9) the integral equation (10) in Ref. [35]. In addition, yet another, even more involved integral equation has been obtained in [35] [see Eq. (5) therein] which has no counterpart in our present context. A possible reason could be that the random matrix ensembles considered in [35] differ from ours in some subtle details. In any case, the derivation of both equations has not been provided in Ref. [35] nor in any subsequent work by these authors [37]. To our knowledge, the first published derivation of (9) is thus contained in the Supplemental Material of Ref. [4].

Incidentally, a predecessor of the integral equation (18) can already be found in Wigner's seminal investigations [25, 26] of banded perturbation matrices whose entries have constant amplitude but random signs. In particular, with the definition $p(z) := iG(z)$, Eqs. (9a) and (9b) in [26] correspond to our Eq. (18) for a step profile $f(x) = q\Theta(1 - x^2)$.

A special case of the present banded random matrix model was adopted by Genway et al. in Ref. [6], investigating the particular setup of a small system in contact with a large heat bath, and focusing on the temporal relaxation behavior of the small system. Formally, the

matrix elements V_{mn}^0 were introduced as independent, unbiased Gaussian random variables with variance (5) and a step profile $f(x) = \alpha\Theta(\Delta_v^2 - x^2)$, even though the effective structure is slightly distorted due to the employed Dyson Brownian motion approach [38] to approximately compute the eigenvector overlap moments which are needed in (92) and (93) [6]. In this setting, Genway et al. then obtained an approximate prediction for the time dependence of the subsystem's reduced density matrix which resembles our present results (7)–(9) [being asymptotically exact, as explained below Eq. (7)]. Notably, they conclude that the coupling to the bath (which is the perturbation in the setup of their work) modifies the isolated reference dynamics by a characteristic damping function which is approximately Gaussian for times $t < \Delta_v^{-1}$ and crosses over to an exponential shape thereafter; we had already briefly commented on this transition in Sec. V below Eq. (91).

Yet another approximation in terms of projection operator techniques is due to Richter et al. [39], adopting a quite similar (non-rigorous) line of reasoning as in Sec. VIA, and indeed arriving at a result of the same formal structure as in (97), except that the function $\tilde{g}(t)$ is now defined somewhat differently, and that the admitted initial states $\rho(0)$ must satisfy certain additional restrictions.

As announced in Sec. VIA, the fact that all those diverse approaches and approximation schemes of varying degree of rigor often lead to quite similar conclusions indicates an astonishing structural stability of the problem and underpins its fundamental nature. Nevertheless, an entirely satisfying treatment can apparently not reasonably circumvent such quite sophisticated and technically involved calculations as those elaborated in Ref. [4].

VII. COMPARISON WITH NUMERICAL EXAMPLES

So far, our main predictions (7), (16) amount to quite well controlled analytical approximations regarding the vast majority of all members of a given random matrix ensemble of perturbations. But what are their implications regarding the “true” (non-random) perturbation when dealing with some specific physical model in (1)?

Similarly as when comparing “true” random numbers with numerically generated pseudo-random numbers, it is in general very difficult to decide whether or not the “true” perturbation V in any concrete physical model can be reasonably well captured by such a random matrix approach. Indeed it may seem *a priori* almost obvious that the true perturbation matrix is not a random matrix. On the other hand, the following counter-argument is equally obvious: Let us assume that the matrix in question is of large but finite dimension and that each matrix element can in principle assume a large but finite number of different possible values. (Such a simplification does not seem to entail very serious problems, since it is unavoidable

able in any numerical treatment.) Sampling each possible value of the matrix elements with some finite probability then gives rise to an ensemble of random matrices, which also contains the “true” perturbation as one of its members. In particular, if the ensemble imitates some key features like sparsity, banded matrix structure etc. of the true perturbation reasonably well, and if we are able to make a statement which applies to the overwhelming majority of all the members of the ensemble (as in our present case), then there is good reason to believe that this statement should also apply to the true perturbation (see also Introduction). Yet, this counter-argument can again be countered as follows: If the statement in question quantitatively depends on certain finer details of the considered ensemble, then the “true” perturbation can at most belong to the vast majority of one ensemble, while it must belong to the tiny minority of all other ensembles. In other words, the previous argument that the true perturbation is realized with some reasonable probability is not yet sufficient to guarantee that it belongs to the majority of all the similarly behaving members of a given ensemble. Again, this objection is mitigated in our present case by the fact that the prediction (7), (16) only depends on two basic parameters of the considered ensemble, i.e., many different ensembles effectively behave in the same way.

As usual in random matrix theory (see also Introduction), the only really convincing way out is to compare our predictions (7), (16) with the actual behavior of concrete examples.

A. Fermionic Hubbard model

As a first example, we consider a variant of the fermionic Hubbard model for which Balzer et al. obtained the perturbed relaxation dynamics numerically in Ref. [40]. A comparison with the typicality prediction from Ref. [4] had already been included in the Supplemental Material there, and we conjectured that visible deviations for short times and larger perturbation strengths are caused by a banded structure of the perturbation matrix V_{mn}^0 . Accordingly, we now employ our refined analytical prediction (7) with $g(t)$ from (16), which explicitly accounts for effects of a decaying perturbation profile via the parameter Δ_v , to further examine this conjecture.

The considered model is defined on a Bethe lattice of infinite coordination number so that H_0 and V in (1) can be written as

$$H_0 := - \sum_{\langle ij \rangle, \sigma} c_{i\sigma}^\dagger c_{j\sigma}, \quad V := \sum_i (n_{i\uparrow} - \frac{1}{2})(n_{i\downarrow} - \frac{1}{2}) \quad (98)$$

using the fermionic creation and annihilation operators $c_{i\sigma}^\dagger$ and $c_{i\sigma}$, respectively, for particles of spin $\sigma \in \{\uparrow, \downarrow\}$ on site i , $n_{i\sigma} := c_{i\sigma}^\dagger c_{i\sigma}$, and $\langle ij \rangle$ to denote connected sites i and j . Initially, every site is occupied by exactly

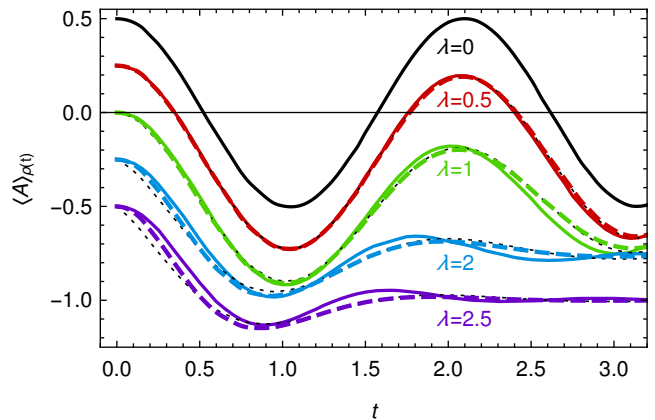


FIG. 6: Time-dependent expectation values of the momentum mode correlation (99) for the fermionic Hubbard model from (98) with various coupling strengths λ , and with a Néel state as initial condition. Solid: DMFT results as published in Fig. 3(a) of Ref. [40]. Dashed: Theoretical prediction (7) using the numerical result (solid black $\lambda = 0$ curve) for the unperturbed $\langle A \rangle_{\rho_0(t)}$, $\langle A \rangle_{\bar{\rho}} = 0$, and $g(t)$ from (16) with $\alpha = 0.045$ and $\Delta_v = 4.88$. Dotted: Same but employing for $g(t)$ the approximation from (45) with $\alpha = 0.035$. Data for finite λ are shifted vertically in steps of -0.25 for better visibility.

one fermion with opposing spins between connected sites (Néel state). Time-dependent expectation values for the observable

$$A := \frac{1}{2} \left(\hat{c}_k^\dagger \hat{c}_{\bar{k}} + \hat{c}_{\bar{k}}^\dagger \hat{c}_k \right), \quad (99)$$

which quantifies correlations between conjugated momentum modes k and \bar{k} as detailed in [40], were calculated for various coupling strengths λ using dynamical mean-field theory (DMFT), and are displayed as solid lines in Fig. 6.

In order to compare these numerical findings with our analytical prediction (7), we take the numerically obtained reference dynamics $\langle A \rangle_{\rho_0(t)}$ ($\lambda = 0$ in Fig. 6) and the long-time asymptotics $\langle A \rangle_{\bar{\rho}} = 0$ as “given”. For the function $g(t)$ from (16), we need the numerical values of the parameters Δ_v from (13) and α from (12). In principle, they can be extracted directly from the empirical variances (5) of the operator V from (98) (see Sec. VII B and Ref. [19] for an example where this analysis is explicitly employed). For the present system, unfortunately, these values are not available from Ref. [40], so we treat them as fit parameters, yielding the dashed curves in Fig. 6. Using the corresponding best fits $\alpha = 0.045$ and $\Delta_v = 4.88$ one furthermore finds with Eqs. (84) and (91) that $\lambda_c \simeq 4.7$ and $t_c \simeq 0.64$.

For comparison, we also show in Fig. 6 as dotted curves the prediction of the simpler approximation (45) for $g(t)$ with only one fit parameter α . This approximation was employed previously in Ref. [4], and is *de facto* restricted – as pointed out below (83) and above (91) – to small coupling strengths λ , or large band widths Δ_v , or large

times t , while otherwise the two-parameter approximation (16) should be better. Fig. 6 indeed confirms our theoretical prediction that the improved approximation (dashed lines) works notably better than the simple approximation (dotted lines) when $t < t_c \simeq 0.64$, albeit there still remain some noticeable deviations from the numerics (solid lines) for large λ - and moderate t -values (for very small and large t -values good agreement is found for rather trivial reasons). These deviations are probably due to the fact that for too strong perturbations the assumption below (3) regarding the mean level spacing may easily be violated: Either the system's energy distribution may no longer be sufficiently sharply peaked, or the mean level spacing itself may be notably changed by the perturbation.

Furthermore, the remaining differences between the solid and dashed lines in Fig. 6 may possibly be attributed to finite size effects (see below Eq. (7)) and the effective approximation of the “true” perturbation profile (5) by the Breit-Wigner form (19), or they may indicate that the specific model Hamiltonian at hand indeed exhibits some non-negligible deviations from the vast majority of the typical members for any of the random matrix ensembles admitted by our present approach (see beginning of this section).

While it may not be overly surprising that a two-parameter fit performs better than a one-parameter fit to approximate the actual dynamics, it is still worth pointing out that the improvement of the two-parameter approximation (16) primarily concerns the regime of larger λ and small t , which is precisely the region where it is anticipated to enhance the prediction (see also Secs. IV and V). For smaller values of λ or larger t , in turn, both approximations essentially agree (cf. Fig. 6).

As an aside we note that any given random matrix ensemble entails a unique value of the parameter α in (12). The fact that the fitted α values notably differ for the two above mentioned approximations may be considered as yet another signature of the fact that the simpler approximation (dotted lines) indeed misses some relevant feature of the true system, namely the banded matrix structure of the perturbation.

A noteworthy final remark is that in the above example the unperturbed expectation value does not approach a constant long-time limit (the unperturbed system does not equilibrate nor thermalize), but rather keeps oscillating forever, and that our theory also admits such cases (as announced in Sec. II).

B. Two-dimensional spin-1/2 lattice

As our second example, we consider a two-dimensional spin- $\frac{1}{2}$ lattice of dimensions $L \times L$, in which the unperturbed Hamiltonian H_0 couples nearest neighbors via isotropic Heisenberg interactions (open boundary condi-

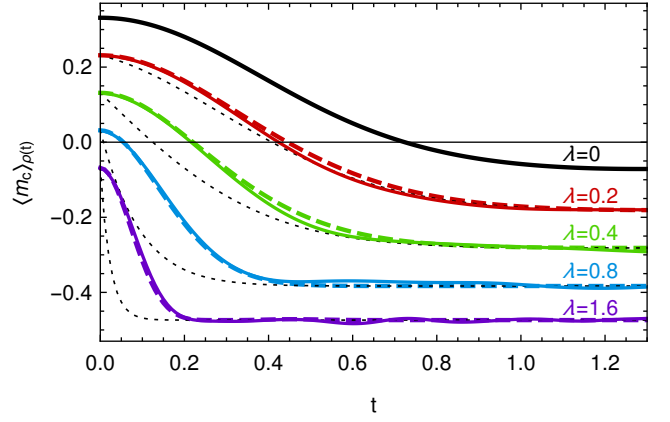


FIG. 7: Time-dependent expectation values of the central magnetization correlation $A = m_c$ from (103) for the 4×4 spin- $\frac{1}{2}$ lattice model from (100)–(101). The initial state is given by $\rho(0) = |\psi\rangle\langle\psi|$ with $|\psi\rangle$ from (102). Solid: Numerical results obtained by exact diagonalization. Dashed: Theoretical prediction (7) using the numerical result (solid black $\lambda = 0$ curve) for the unperturbed $\langle A \rangle_{\rho_0(t)}$, the numerically determined $\langle A \rangle_{\bar{\rho}} = -0.0896, -0.0820, -0.0830, -0.0738$ for $\lambda = 0.2, 0.4, 0.8, 1.6$, respectively, and $g(t)$ from (16) with $\alpha = 2.64$ and $\Delta_v = 7.32$ [see below Eq. (101)]. Dotted: Same but employing for $g(t)$ the approximation from (45). Data for finite λ are shifted vertically in steps of -0.1 .

tions),

$$H_0 := \sum_{i,j=1}^L \boldsymbol{\sigma}_{i,j} \cdot (\boldsymbol{\sigma}_{i+1,j} + \boldsymbol{\sigma}_{i,j+1}), \quad (100)$$

while the perturbation provides an additional coupling of next-nearest neighbors via spin-flip terms with respect to the z direction,

$$V := \sum_{i,j=1}^{L-1} \sum_{\alpha=x,y} (\sigma_{i,j}^{\alpha} \sigma_{i+1,j+1}^{\alpha} + \sigma_{i+1,j}^{\alpha} \sigma_{i,j+1}^{\alpha}). \quad (101)$$

Here $\boldsymbol{\sigma}_{i,j} := (\sigma_{i,j}^x, \sigma_{i,j}^y, \sigma_{i,j}^z)$ is a vector of Pauli matrices acting on site (i, j) . For a lattice with $L = 4$, the corresponding perturbation profile $\sigma^2(x)$ from (5) was computed numerically using exact diagonalization in Ref. [19], yielding $\alpha = 2.64$ and $\Delta_v = 7.32$ within an energy window from $E = -8.8$ to 5.8 . The associated crossover coupling from (84) is thus $\lambda_c \simeq 0.75$, and the crossover time from (91) is $t_c \simeq 0.43$.

We prepare the system in the state $\rho(0) = |\psi\rangle\langle\psi|$ with

$$|\psi\rangle \propto e^{-H_0^2/2\Delta^2} \sigma_{2,2}^+ \sigma_{3,3}^+ |\phi\rangle, \quad (102)$$

where $\Delta = 2$, $\sigma_{i,j}^+ := \sigma_{i,j}^x + i\sigma_{i,j}^y$, and $|\phi\rangle$ denotes a Haar-distributed random vector in the Hilbert space sector with vanishing total magnetization in the z direction. This emulates a system in thermal equilibrium at infinite temperature, for which the spins at sites $(2, 2)$ and $(3, 3)$

are prepared in the “up” state, followed by a macroscopic energy measurement yielding $E = 0$.

Starting from this state, we monitor the correlation between the z magnetization of the two initially deflected sites,

$$m_c := \sigma_{2,2}^z \sigma_{3,3}^z. \quad (103)$$

The numerically obtained time-dependent expectation values are shown as solid lines in Fig. 7 for various values of the coupling strength λ , spanning the entire regime from weak perturbations ($\lambda < \lambda_c$) to moderately strong perturbations ($\lambda > \lambda_c$).

To compare our analytical prediction (7), we adopt the function $g(t)$ from (16) with the known values $\alpha = 2.64$ and $\Delta_v = 7.32$ [see below Eq. (101)] and the numerically available expectation values $\langle A \rangle_{\bar{\rho}}$ (cf. figure caption). This leads to the dashed curves in Fig. 7, which are in remarkable agreement with the numerical results. Notably, there are no free fit parameters in this example, all quantities entering the prediction (7), (16) are available directly via a numerical analysis of H_0 and V from (100) and (101), respectively.

In addition, we also display the prediction (7) with the weak-perturbation and long-time asymptotics (45) for $g(t)$ by the dotted lines in Fig. 7. This approximation indeed works in the expected regimes ($\lambda \ll \lambda_c$ or $t \gg t_c$), but obviously fails for other combinations of λ and t , highlighting the substantial improvement of the theory resulting from the refined expression (16) for $g(t)$.

C. Spin-1/2 XXX ladder

Our third example consist in a spin- $\frac{1}{2}$ ladder model, where H_0 and V in (1) are given by

$$H_0 := \sum_{l=1}^L \sum_{k=1}^2 \mathbf{S}_{l,k} \cdot \mathbf{S}_{l+1,k}, \quad V := \sum_{l=1}^L \mathbf{S}_{l,1} \cdot \mathbf{S}_{l,2}. \quad (104)$$

Here $\mathbf{S}_{l,k} = \boldsymbol{\sigma}_{l,k}/2$ denote standard spin- $\frac{1}{2}$ operators acting on site (l, k) . The reference system \bar{H}_0 thus consists of two spin chains (or “legs”) of length L with nearest-neighbor Heisenberg interactions, and the perturbation V couples them via Heisenberg terms as well. In other words, this model exemplifies a case of two isolated many-body subsystems, brought into contact by the perturbation V (see Sec. II).

Richter et al. studied in Ref. [39] the current autocorrelation function $C(t) := \text{Tr}\{\rho_{\text{eq}} e^{iHt} J e^{-iHt} J\}/L$ of this model, where ρ_{eq} denotes the canonical density operator at infinite temperature (thus proportional to the identity operator), and where

$$J := \sum_{l=1}^L \sum_{k=1}^2 \left(S_{l,k}^x S_{l+1,k}^y - S_{l,k}^y S_{l+1,k}^x \right) \quad (105)$$

is the spin current along the legs. Within the dynamical typality framework they utilized to simulate $C(t)$ [39],

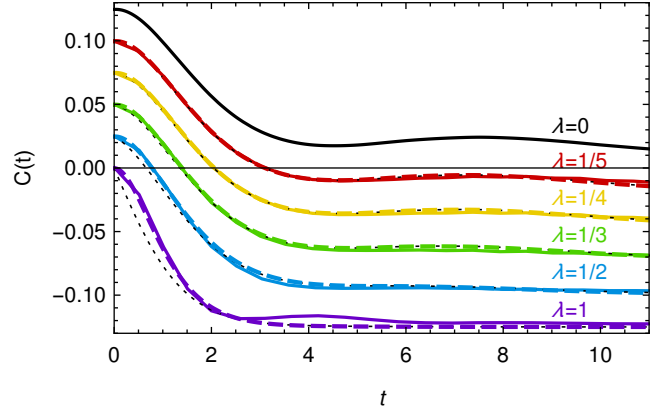


FIG. 8: Time-dependent expectation values of the current correlation function $C(t) = \text{Tr}[\rho_{\text{eq}} e^{iHt} J e^{-iHt} J]/L = \langle J \rangle_{\rho(t)}$ (see also main text) for the spin ladder model (104). Solid: Numerical results as provided in Fig. 2(c) of Ref. [39]. Dashed: Theoretical prediction (7) using the numerical result (solid black $\lambda = 0$ curve) for the unperturbed $\langle J \rangle_{\rho_0(t)}$, $\langle J \rangle_{\bar{\rho}} = 0$, and $g(t)$ from (16) with $\alpha = 0.13$ and $\Delta_v = 3.26$. Dotted: Same but employing for $g(t)$ the approximation from (45) with $\alpha = 0.11$. Data for finite λ are shifted vertically in steps of -0.025 for better visibility.

and exploiting the fact that $\text{Tr}\{J\} = 0$, the autocorrelation function $C(t)$ from above can be rewritten in the form $\langle J \rangle_{\rho(t)}$ (cf. Eq. (2)) with initial state $\rho(0) = |\psi\rangle\langle\psi|$, where $|\psi\rangle$ is chosen proportional to $\sqrt{1 + J/L} |\phi\rangle$ [41], and $|\phi\rangle$ being a state drawn at random from the pertinent Hilbert space according to the Haar measure [39].

The numerical results for $C(t) = \langle J \rangle_{\rho(t)}$ from Ref. [39] are depicted as solid lines in Fig. 8. We compare them to our theory (7), (16) by exploiting $\langle J \rangle_{\bar{\rho}} = 0$ (thermal long-time asymptotics) and fitting the parameters α and Δ_v since – as in the previous example from Sec. VII A – their precise numerical values are not available. (We remark that the authors of [39] do explore the structure of their perturbation matrix V_{mn}^0 , but for a smaller system size than in Fig. 8, and indeed find a banded and sparse structure in qualitative agreement with our setup. Unfortunately, the precise scaling of the parameters α and Δ_v with the system size L is unclear, so that it is not possible to extrapolate their quantitative values for the system in Fig. 8 from the available data.) The dashed lines in Fig. 8 represent the so-obtained theoretical predictions with $\alpha = 0.13$ and $\Delta_v = 3.3$, revealing very good agreement with the numerics. Similarly as in the previous example from Sec. VII A, we also included as dotted lines a fit to the simpler approximation from (45), which is expected (and found) to apply when the perturbation is weak, or the band width is large, or the time is large.

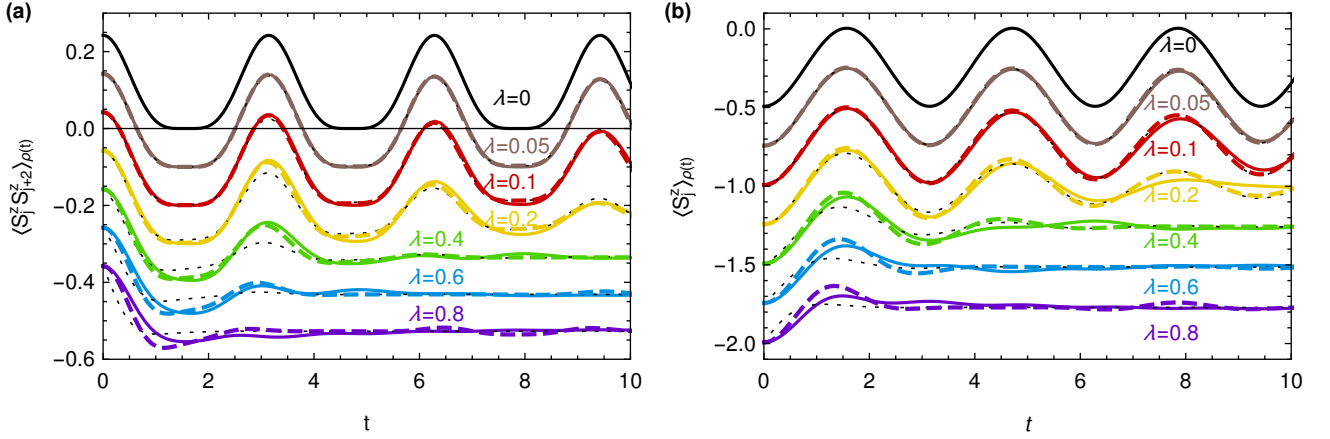


FIG. 9: Time-dependent expectation values of (a) the next-nearest-neighbor correlation $A = S_j^z S_{j+2}^z$ and (b) the transverse magnetization $A = S_j^z$ for the transverse-field Ising model (106) with various coupling strengths λ , and employing the ground state for $\lambda = 4$ as initial condition (quantum quench). Solid: Exact analytical results in the thermodynamic limit $L \rightarrow \infty$. Dashed: Theoretical prediction (7) using the exact result (solid black $\lambda = 0$ curve) for the unperturbed $\langle A \rangle_{\rho_0(t)}$, the exact long-time limit $\langle A \rangle_{\bar{\rho}}$, and $g(t)$ from (16) with $\alpha = 1.1$ and $\Delta_v = 0.22$. [In particular, the same values were used for all dashed curves in (a) and (b).] Dotted: Same but employing for $g(t)$ the approximation from (45) with $\alpha = 0.70$. Data for finite λ are shifted vertically in steps of -0.1 in (a) and -0.25 in (b) for better visibility.

D. Transverse-field Ising model

As a last example, we consider the one-dimensional transverse-field Ising model, whose Hamiltonian is given by (1) with

$$H_0 := -2 \sum_{j=1}^L S_j^x S_{j+1}^x, \quad V := - \sum_{j=1}^L S_j^z, \quad (106)$$

where the $S_j^{x,z}$ are again the standard spin- $\frac{1}{2}$ operators acting on site j modulo L (periodic boundary conditions). Hence, the reference system is the Ising model at vanishing external field, and the perturbation consists of a transverse magnetic field with coupling strength λ . This model is well-known to be integrable for all values of λ .

Specifically, we consider an infinite chain (thermodynamic limit $L \rightarrow \infty$), which is prepared in the ground state of the perturbed Hamiltonian with $\lambda = 4$, and which is subsequently quenched to a Hamiltonian with a smaller λ value. As our first observable, we consider the next-nearest neighbor correlation $S_j^z S_{j+2}^z$ (the choice of j is irrelevant), which is known to be nonthermalizing in the present setup [42]. Our second observable is the transverse magnetization S_j^z . Both observables exhibit permanent oscillations in the reference system H_0 for the chosen initial state, and the expectation-value dynamics can be calculated exactly for all values of λ [43–45].

Similarly as before, we compare in Fig. 9 those numerically exact results (solid lines) to our theory from (7) and (16), employing the exact results also for the reference dynamics $\langle A \rangle_{\rho_0(t)}$ and for the long-time limit $\langle A \rangle_{\bar{\rho}}$, while Δ_v and α are again treated as fit parameters, yielding $\Delta_v = 0.22$ and $\alpha = 1.2$. The improved approximation

(dashed lines) again works notably better than the simple approximation (dotted lines) when $\lambda > \lambda_c \simeq 0.2$.

We also note that – like in the example from Sec. VII A – we are dealing here again with a case for which the unperturbed dynamics does not equilibrate in the long-time limit. Moreover, both the unperturbed and the perturbed systems are now always integrable. Though this does not automatically violate any of the formal requirements (cf. Sec. II), our theory may not have been originally expected to be still applicable in view of the fact that most perturbations of any given ensemble will lead to a non-integrable perturbed Hamiltonian. For the particular combination of observables and initial state from Fig. 9, the presence of an extensive number of conservation laws thus seems to be of subleading importance as far as the dynamical response of the system to the perturbation is concerned.

VIII. CONCLUSIONS

Characterizing the effect of reasonably small perturbations on the behavior of dynamical systems is an important and recurrent task in many areas of physics. The pertinent key contribution of our present work is an analytical prediction of this response in isolated many-body quantum systems based on just two parameters of the perturbation: its overall strength $\alpha\lambda^2$ [Eq. (12)] and its band width Δ_v [Eq. (13)], both of which are derived from the magnitude of the perturbation matrix elements in the eigenbasis of the unperturbed Hamiltonian via (5). The analytical prediction (7) suggests that the perturbed time-dependent expectation values $\langle A \rangle_{\rho(t)}$ of an observable A resemble the unperturbed $\langle A \rangle_{\rho_0(t)}$, but are mod-

ified by a function $g(t)$, specified in (16) and depending on the two perturbation parameters $\alpha\lambda^2$ and Δ_v , which pushes them towards their (perturbed) long-time limit. For late times and/or weak perturbations, these perturbed relaxation characteristics are akin to Fermi's golden rule and in fact comprise the latter as a special case. At the same time, significant deviations from the golden-rule behavior are observed and quantified via (16) for stronger perturbations and short times.

Given its simplicity, the prediction (7), (16) can surely not be expected to hold always and invariably. Naturally, deviations are unsurprising if certain prerequisites of the derivation itself are violated, the most important ones being a well-defined macroscopic energy and a perturbation that is not too strong. However, deviations can also occur in a more subtle manner due to the inherent probabilistic character of our random matrix approach. Moreover, as explained in Sec. VII, it is unfortunately quite hard to determine in general whether a given physical perturbation is a “typical” member of any of the admitted perturbation ensembles.

In any case, a crucial prerequisite is that the chosen ensemble faithfully reproduces the key mechanisms responsible for the modifications in the perturbed system. Here, we identified the perturbation profile $\sigma^2(x)$ from (5) as the key property for the dynamics in a large variety of setups, prominently highlighted by the integro-differential equation (10). Nevertheless, other features such as the locality and few-body character of interactions may become important in other setups, too (see below).

Generally speaking, it is not unusual that the behavior of macroscopic systems can be characterized in terms of just a few parameters, for otherwise we would not be able to describe them theoretically at all. Crucially, the examples from Sec. VII (see also Ref. [4] for further examples) demonstrate that the theory is successful at predicting the dynamical response for a variety of different models and perturbations, and even for systems which cannot really be considered “macroscopic” yet.

Methodologically, our present work builds on the results from Ref. [4], which, in particular, established the general structure (7) for the quantum many-body relaxation under the influence of banded and sparse perturbation matrices. Substantial progress was achieved regarding analytical expressions for the function $g(t)$ governing that perturbed relaxation, culminating in the aforementioned approximation (16) in terms of the perturbation strength $\alpha\lambda^2$ and band width Δ_v . This latter expression originally arises as the second-order approximation for the special choice of a single ($N = 1$) Breit-Wigner perturbation profile (19), for which we were able to solve the underlying integral equation (18) leading to $g(t)$ via (8) exactly in the form of an infinite continued fraction (see Sec. IV). Based on universal limiting expressions for weak and strong perturbations and short and long times as well as numerical explorations, we subsequently argued in Sec. V that the precise form of $g(t)$ is rather insensitive to further perturbation details apart from $\alpha\lambda^2$ and Δ_v ,

finally leading to (16).

Besides our own works [4, 19], similar concepts and ideas have been developed and pursued in various studies by other authors, too, of which we reviewed the most closely related ones known to us in Sec. VI.

An interesting direction for future research is to obtain a better understanding of the features of “real” physical perturbations which may potentially render them atypical with respect to the random matrix ensembles considered here. From a mathematical point of view, these are correlations between the perturbation matrix elements, but how they arise from the geometrical structure and types of interactions [46, 47] and to what extent they matter with respect to the many-body relaxation is still poorly understood.

Acknowledgments

This work was supported by the Deutsche Forschungsgemeinschaft (DFG) within the Research Unit FOR 2692 under Grant No. 397303734, by the Paderborn Center for Parallel Computing (PC²) within the Project HPC-PRF-UBI2, and by the International Centre for Theoretical Sciences (ICTS) during a visit for the program - Thermalization, Many body localization and Hydrodynamics (Code: ICTS/hydrodynamics2019/11).

Appendix A: General properties of $G(z)$

In this appendix we discuss several general issues regarding the solutions $G(z)$ of the non-linear integral equation (9), including existence, uniqueness, symmetries, and the physical origin of this equation.

Generally speaking, statements about the existence and uniqueness of solutions of non-linear integral equations as exemplified by (9) are known to be difficult to obtain.

Before turning to our specific case at hand, it may be worthwhile to recall the following basic facts: The function $f(z) := z^*$ is not analytic for any $z \in \mathbb{C}$ (the Cauchy-Riemann differential equations are always violated). It follows that if $f(z)$ is analytic, then $h(z) := f(z^*)$ is in general no longer analytic, and similarly for $h(z) := [f(z)]^*$. On the other hand, $h(z) := -f(z)$ and $h(z) := f(-z)$ are still analytic, and also $h(z) := [f(z^*)]^*$ is again analytic, and hence also $h(z) := -[f(-z^*)]^*$.

Due to the symmetry (6) of $\sigma^2(x)$, one readily verifies that if $G(z)$ solves the integral equation (9), then there must exist in full generality four solutions of (9), namely (see also (32))

$$G_1(z) := G(z) = v(x, y) + iw(x, y), \quad (A1)$$

$$G_2(z) := -[G(-z^*)]^* = -v(-x, y) + iw(-x, y), \quad (A2)$$

$$G_3(z) := [G(z^*)]^* = v(x, -y) - iw(x, -y), \quad (A3)$$

$$G_4(z) := -G(-z) = -v(-x, -y) - iw(-x, -y). \quad (A4)$$

In general, solutions of the non-linear integral equation (9) thus come in quadruples of the structure (A1)-(A4). However, some of the members of a quadruple may actually coincide, for instance due to symmetry reasons (see below). Moreover, we anticipate that they may exhibit poles (or other singularities), and hence may not be well-defined or may not solve (9) for all $z \in \mathbb{C}$ simultaneously. In the following, we always tacitly focus on one particular such quadruple of solutions.

If $G(z) = G_1(z)$ furthermore satisfies the two additional requirements (i) and (ii) below (20), then one readily verifies also $G_2(z)$ will satisfy the same requirements. On the other hand, $G_3(z)$ and $G_4(z)$ will fulfill two slightly modified requirements, namely the same requirements as below (20) except that they must now apply for all z with $\text{Im}(z) > 0$ (but possibly not any more for all $z \in \mathbb{C}$ with $\text{Im}(z) < 0$).

Under the assumption that the solution of (9), in conjunction with the two requirements below (20), is unique, it follows that $G_2(z) = G_1(z)$, and hence $G(z) = G_1(z)$ must satisfy the symmetry property (31). Incidentally, also the two remaining solutions $G_3(z)$ and $G_4(z)$ then actually must coincide and exhibit the same symmetry (31).

Further insight regarding those existence and uniqueness issues seems hardly possible on the basis of the integral equation (9) alone. Rather, it seems indispensable to also take into account the origin of this equation in the derivation of the final result (7). Referring to [4] for more details, a suitable starting point is the following implicit definition of the function $u(E)$:

$$[|U_{mn}|^2]_V = u(E_m^0 - E_n^0) , \quad (\text{A5})$$

where, as in the main paper, U_{mn} are the overlaps of the perturbed and unperturbed eigenstates from (4) and where $[\cdots]_V$ indicates the average over the considered ensemble of perturbations V . For the rest, everything is very similar to the implicit definition of the function $\sigma^2(x)$ in (5). The existence and uniqueness of this function $u(E)$ may thus be taken for granted. Moreover, by means of our usual approximation $E_m^0 - E_n^0 \simeq (m - n)\varepsilon$ (see above (5)), the following two properties readily follow from the definition (A5):

$$u(E) \geq 0 , \quad (\text{A6})$$

$$\int dE u(E) = \varepsilon . \quad (\text{A7})$$

The key point of the derivation of the final result (7) in Ref. [4] is the following relation between the functions $u(E)$ and $G(z)$:

$$u(E) = \frac{\varepsilon}{\pi} \lim_{\eta \downarrow 0} \text{Im} G(E - i\eta) , \quad (\text{A8})$$

where $G(z)$ must solve the non-linear integral equation (9). On the other hand, $G(z)$ originally arises [4] as an ensemble average of the form $[\mathcal{G}(z)]_V = G(z - H_0)$,

where $\mathcal{G}(z) := (z - H)^{-1}$ is the resolvent or Green's function of the perturbed Hamiltonian H in (1), see also below (8). For the sake of clarity, we temporarily denote this specific (original) function as $\tilde{G}(z)$, to better distinguish it from all the possibly existing further solutions of the non-linear integral equation (9). Taking for granted that the entire derivation in [4] is sound, it follows that this ensemble-averaged (scalar) resolvent $\tilde{G}(z)$ exists, is unique, and solves (9). Moreover, one can infer from the above definitions that the Hermiticity of $\mathcal{G}(z)$ implies $\tilde{G}(z^*) = [\tilde{G}(z)]^*$, and that $\tilde{G}(z)$ must in general be expected to exhibit non-analyticities along the real axis [4]. In contrast, the (exact or approximate) solutions we encountered in the main paper usually do not exhibit the symmetry $G(z^*) = [G(z)]^*$, and instead are often analytic on the real axis. Put differently, the essential difference between our solutions $G(z)$ and the original $\tilde{G}(z)$ is that $G(z)$ initially was obtained in the main paper as a solution of the non-linear integral equation (9) on the complex half-plane \mathbb{C}^- from (20), and subsequently was extended as far as possible (i.e. up to poles) by analytic continuation. On the other hand, $\tilde{G}(z)$ may be imagined to arise in the same way as a solution of (9) on the half-plane \mathbb{C}^- , but then is already fixed also for the remaining arguments z via $\tilde{G}(z^*) = [\tilde{G}(z)]^*$. In other words, if $\tilde{G}(z)$ agrees with $G(z)$ in (A1) on \mathbb{C}^- , then $\tilde{G}(z)$ will be given by $G_3(z)$ from (A3) for the remaining arguments z . [In particular, $\tilde{G}(z)$ thus still solves the non-linear integral equation (9) for all $z \in \mathbb{C} \setminus \mathbb{R}$.]

Let us now assume that we obtained a quadruple of solutions (A1)-(A4), and one of them, say $G_1(z)$, leads via (A8) to a function $u(E)$ which satisfies (A6) and (A7). Then the same applies for the corresponding function $u(E)$ deriving from $G_2(z)$. On the other hand, $G_3(z)$ and $G_4(z)$ will entail functions $u(E)$ via (A8) which violate (A6) and (A7) (or they are not well-defined for the arguments z required in (A8) in the first place). Hence, one of the first two solutions is expected to be the physically relevant one (i.e. to agree with $\tilde{G}(z)$ on \mathbb{C}^-), while the last two solutions must be excluded as unphysical.

All these arguments strongly suggest (but still do not prove), that a solution $G(z)$ of the non-linear integral equation (9), for which $u(E)$ from (A8) moreover satisfies (A6) and (A7), exists and is unique. Furthermore, the uniqueness strongly suggests that also the symmetry property (31) will be fulfilled. According to (32), (34), and (A8) it then also follows that $u(E)$ must be an even function of E ,

$$u(-E) = u(E) . \quad (\text{A9})$$

All these properties were indeed recovered in all our particular (possibly approximate and either analytical or numerical) solutions $G(z)$ from the main paper. [Note that (A7) is in fact equivalent to (42) due to (A8) and (8).]

Appendix B: Convergence of Eq. (30)

In this appendix, we show that the infinite continued-fraction representation of $H(z)$ from Eq. (30) converges for all $z \in \mathbb{C}$ with $\text{Re}(z) > 0$ and any given $\beta \in \mathbb{R}^+$. Introducing the notation

$$\mathcal{K}_{k=0}^{\infty} \frac{a_k}{b_k} := \frac{a_0}{b_0 + \frac{a_1}{b_1 + \frac{a_2}{b_2 + \dots}}} \quad (\text{B1})$$

for the infinite continued fraction with coefficients $a_k, b_k \in \mathbb{C}$, we can express $H(z)$ in (30) as

$$H(z) = \frac{1}{\beta} \mathcal{K}_{k=0}^{\infty} \frac{\beta}{z+k}. \quad (\text{B2})$$

We also define the auxiliary continued fractions

$$h_n(z) := \mathcal{K}_{k=n}^{\infty} \frac{\beta}{z+k}. \quad (\text{B3})$$

Provided that $h_{n+1}(z)$ converges for given n , Eq. (B2) can then be written as

$$H(z) = \frac{1}{\beta} \mathcal{K}_{k=0}^n \frac{\beta}{z+k+\delta_{nk}h_{n+1}(z)}, \quad (\text{B4})$$

i.e., as a finite continued fraction of order n with the “rest” $h_{n+1}(z)$ appended to the denominator of the last term.

Restricting ourselves to $\text{Re}(z) > 0$ and recalling that $\beta > 0$, it therefore suffices to show that, for fixed z , there exists $n_0 \in \mathbb{N}$ such that $h_{n_0}(z)$ is convergent because the denominators of all finite fractions in (B4) have a strictly positive real part and thus cannot develop poles.

The existence of such n_0 for any preset $z = x + iy$ with $x > 0$ and $y \in \mathbb{R}$ follows directly from the Ślezyński-Pringsheim theorem [48], which states that the infinite continued fraction (B3) converges if $|z+k| \geq \beta+1$ for all $k \geq n$. If $|z| \geq \beta+1$, we can thus readily conclude that $h_n(z)$ converges for all n . Otherwise, the theorem assures convergence of $h_n(z)$ for all $n \geq n_0$ with

$$n_0 := \left\lceil \sqrt{(\beta+1)^2 - y^2} - x \right\rceil, \quad (\text{B5})$$

where $\lceil x \rceil$ denotes the smallest integer greater than or equal to x (“ceiling function”).

Appendix C: Various representations of $g(t)$

In this appendix, we derive several alternative equations for the function $g(t)$ from (8) under the assumption that $G(z)$ fulfills the requirements (i) and (ii) below (20). In particular, the integral equation (10) for $g(t)$ is obtained. Moreover, it is shown that $g(t)$ can be written in the form (35) provided $G(z)$ exhibits the symmetry property (31).

Representing $\text{Im } G(E - i\eta)$ as $[G(E - i\eta) - G^*(E - i\eta)]/2i$, the function $g(t)$ from (8) can be rewritten in the form

$$g(t) = \lim_{\eta \downarrow 0} g_{\eta}(t), \quad (\text{C1})$$

$$g_{\eta}(t) := \frac{\tilde{g}_{\eta}(t) - \tilde{g}_{\eta}^*(-t)}{2\pi i} \quad (\text{C2})$$

$$\tilde{g}_{\eta}(t) := \int dE e^{iEt} G(E - i\eta). \quad (\text{C3})$$

In particular, taking for granted that the integral on the right hand side of (8) exists, also the existence of the Fourier transform (C3) should not be a problem [49].

From (C1) and (C2) we can conclude that

$$g(-t) = g^*(t), \quad (\text{C4})$$

and with (A7), (A8) that

$$g(0) = 1. \quad (\text{C5})$$

In doing so, we thus tacitly take for granted the relations (A7) and (A8). Alternatively, (C5) is also recovered as the limit of $g(t)$ for asymptotically small t in all specific examples known to us, see also Eq. (42) in the main text.

In view of (C4) and (C5), we can and will mostly focus on $t > 0$ from now on.

Taking for granted that $G(z)$ fulfills the assumptions (i) and (ii) below (20), standard residue methods imply that $\tilde{g}_{\eta}(t)$ in (C3) must vanish for $t < 0$ implying with (C2) that

$$g_{\eta}(t) = \tilde{g}_{\eta}(t)/2\pi i \quad \text{for } t > 0. \quad (\text{C6})$$

With (C1) and (C3), we thus obtain

$$g(t) = \frac{1}{2\pi i} \lim_{\eta \downarrow 0} \int dx G(x - i\eta) e^{ixt} \quad \text{for } t > 0. \quad (\text{C7})$$

If $G(z)$ in addition satisfies the symmetry property (31), one can infer from (C3) that $\tilde{g}_{\eta}^*(t) = -\tilde{g}_{\eta}(t)$. With (C1) and (C2) it follows that $g(-t) = g(t)$ and with (C4) that $g(t) = g^*(t)$ for all t . Exploiting (C7) we thus recover (35), at least for all $t \neq 0$. In the remaining case $t = 0$, (35) follows by continuation or from (A7) and (A8), see also the discussion below (C5).

In the following we no longer require that $G(z)$ exhibits the symmetry property (31). Next, we observe that the integral equation (18) can be rewritten by choosing $z = E - i\eta$ and setting $h(E) := G(E - i\eta)$ in the form

$$[E - i\eta] h(E) - h(E) \int dx h(E - x) f(x) = 1. \quad (\text{C8})$$

Upon multiplying this equation by e^{iEt} , integrating over E , exploiting that $\int dE e^{iEt} h(E) = \tilde{g}_{\eta}(t)$ according to (C3), and applying textbook Fourier transformation methods, a straightforward but somewhat tedious calculation yields

$$\frac{\dot{\tilde{g}}_{\eta}(t)}{i} - i\eta \tilde{g}_{\eta}(t) - \int \frac{ds}{2\pi} \tilde{g}_{\eta}(t-s) \tilde{g}_{\eta}(s) \tilde{f}(s) = 2\pi \delta(t), \quad (\text{C9})$$

where $\tilde{f}(t)$ is the Fourier transform of $f(x)$ from (86). Focusing on $t > 0$ and utilizing under the integral in (C8) that $\tilde{g}_\eta(t) = 0$ for $t < 0$ (see above (C6)), we can conclude that

$$\dot{\tilde{g}}_\eta(t) + \eta \tilde{g}_\eta(t) + \int_0^t \frac{ds}{2\pi i} \tilde{g}_\eta(t-s) \tilde{g}_\eta(s) \tilde{f}(s) = 0 \quad (\text{C10})$$

for $t > 0$. With (C6) and (C1) this finally yields

$$\dot{g}(t) + \int_0^t ds g(t-s) g(s) \tilde{f}(s) = 0 \quad (\text{C11})$$

for $t > 0$. Formally, this amounts to an initial value problem for $g(t)$ with initial condition (C5). The solution for negative t then follows from (C4), and can be shown to still satisfy (C11). In other words, (C11) in fact applies for arbitrary t , i.e., we recover Eq. (10) from the main text.

-
- [1] F. Haake, *Quantum Signatures of Chaos* (Springer, Berlin, 2010).
- [2] N. G. van Kampen, The case against linear response theory. *Phys. Norv.* **5**, 279 (1971).
- [3] T. A. Brody, J. Flores, J. B. French, P. A. Mello, A. Pandey, and S. S. M. Wong, Random-matrix physics: spectrum and strength fluctuations, *Rev. Mod. Phys.* **53**, 385 (1981).
- [4] L. Dabelow and P. Reimann, Relaxation Theory for Perturbed Many-Body Quantum Systems versus Numerics and Experiment, *Phys. Rev. Lett.* **124**, 120602 (2020).
- [5] J. M. Deutsch, Quantum statistical mechanics in a closed system, *Phys. Rev. A* **43**, 2046 (1991).
- [6] S. Genway, A. F. Ho, and D. K. K. Lee, Dynamics of thermalization and decoherence of a nanoscale system, *Phys. Rev. Lett.* **111**, 130408 (2013).
- [7] C. Nation and D. Porras, Quantum chaotic fluctuation-dissipation theorem: effective Brownian motion in closed quantum systems, *Phys. Rev. E* **99**, 052139 (2019).
- [8] S. Goldstein, J. L. Lebowitz, R. Tumulka, and N. Zanghì, Long-Time Behavior of Macroscopic Quantum Systems: Commentary Accompanying the English Translation of John von Neumann's 1929 Article on the Quantum Ergodic Theorem, *Eur. Phys. J. H* **35**, 173 (2010).
- [9] S. Goldstein, J. L. Lebowitz, C. Mastrodonato, R. Tumulka, and N. Zanghì, On the Approach to Thermal Equilibrium of Macroscopic Quantum Systems, *Phys. Rev. E* **81**, 011109 (2010).
- [10] C. Gogolin and J. Eisert, Equilibration, thermalization, and the emergence of statistical mechanics in closed quantum systems, *Rep. Prog. Phys.* **79**, 056001 (2016).
- [11] L. D'Alessio, Y. Kafri, A. Polkovnikov, and M. Rigol, From Quantum Chaos and Eigenstate Thermalization to Statistical Mechanics and Thermodynamics, *Adv. Phys.* **65**, 239 (2016).
- [12] T. Mori, T. N. Ikeda, E. Kaminishi, and M. Ueda, Thermalization and prethermalization in isolated quantum systems: a theoretical overview, *J. Phys. B* **51**, 112001 (2018).
- [13] F. Borgonovi, F. M. Izrailev, L. F. Santos, and V. G. Zelevinsky, Quantum chaos and thermalization in isolated systems of interacting particles, *Phys. Rep.* **626**, 1 (2016).
- [14] R. Nandkishore and D. A. Huse, Many-body localization and thermalization in quantum statistical mechanics, *Annu. Rev. Condens. Matter Phys.* **6**, 15 (2015).
- [15] T. Langen, T. Gasenzer, and J. Schmiedmayer, Prethermalization and universal dynamics in near-integrable quantum systems, *J. Stat. Mech.* **2016**, 064009 (2016).
- [16] H. Tasaki, Typicality of Thermal Equilibrium and Thermalization in Isolated Macroscopic Quantum Systems, *J. Stat. Phys.* **163**, 937 (2016).
- [17] P. Reimann, Eigenstate thermalization: Deutsch's approach and beyond, *New J. Phys.* **17**, 055025 (2015).
- [18] C. Nation and D. Porras, Off-diagonal observable elements from random matrix theory: distributions, fluctuations, and eigenstate thermalization, *New. J. Phys.* **20**, 103003 (2018).
- [19] L. Dabelow, P. Vorndamme, and P. Reimann, Modification of quantum many-body relaxation by perturbations exhibiting a banded matrix structure, *Phys. Rev. Research* **2**, 033210 (2020).
- [20] To recover this conclusion within our present formalism, we note that a large band width in (80) is tantamount to large a_n -values (see also (19)). On the other hand, the small- β asymptotics in (62)-(77) requires that the \tilde{a}_n 's are kept fixed while the β_n 's must become small. This is achieved by rewriting (60) and (61) as $a_n = a\tilde{a}_n$ and $\beta_n = \tilde{f}_n\tilde{a}_n/a$, keeping the \tilde{a}_n (and also the \tilde{f}_n) fixed, and letting a grow. Hence, the band width in (80) now indeed grows linearly with a , while β in (81) decreases as $1/a$ (see also (27)).
- [21] J. J. Sakurai, *Modern Quantum Mechanics* (Addison-Wesley, Reading, MA, 1994).
- [22] K. Mallayya, M. Rigol, and W. De Roeck, Prethermalization and Thermalization in Isolated Quantum Systems, *Phys. Rev. X* **9**, 021027 (2019).
- [23] J. M. Deutsch, A closed quantum system giving ergodicity, <https://deutsch.physics.ucsc.edu/pdf/quantumstat.pdf> (unpublished).
- [24] G. Ithier and S. Ascroft, Statistical diagonalization of a random biased Hamiltonian: the case of the eigenvectors, *J. Phys. A: Math. Theo.* **51**, 48LT01 (2018).
- [25] E. P. Wigner, Characteristic vectors of bordered matrices with infinite dimensions, *Ann. Math.* **62**, 548 (1955).
- [26] E. P. Wigner, Characteristic Vectors of Bordered Matrices with Infinite Dimensions II, *Ann. Math.* **65**, 203 (1957).
- [27] A. D. Mirlin and Y. V. Fyodorov, Universality of level correlation function of sparse random matrices, *J. Phys. A: Math. Gen.* **24**, 2273 (1991).
- [28] M. Wilkinson, M. Feingold, and D. M. Leitner, Localization and spectral statistics in banded random matrix

- ensembles, J. Phys. A: Math. Gen. **24**, 175 (1991).
- [29] K. Życzkowski, M. Levenstein, M. Kuś, and F. Izrailev, Eigenvector statistics of random band matrices, Phys. Rev. A **45**, 811 (1992).
 - [30] T. Prosen and M. Robnik, Energy level statistics and localization in sparsely banded random matrix ensemble, J. Phys. A: Math. Gen. **26**, 1105 (1993).
 - [31] P. Jacquod and D. L. Shepelyansky, Hidden Breit-Wigner Distribution and Other Properties of Random Matrices with Preferential Basis, Phys. Rev. Lett. **75**, 3501 (1995).
 - [32] Y. V. Fyodorov and A. D. Mirlin, Statistical properties of random banded matrices with strongly fluctuating diagonal elements, Phys. Rev. B **52**, R11580 (1995).
 - [33] G. Casati, B. V. Chirikov, I. Guarneri, and F. M. Izrailev, Quantum ergodicity and localization in conservative systems: the Wigner band random matrix model, Phys. Lett. A **223**, 430 (1996).
 - [34] D. Shlyakhtenko, Random Gaussian Band Matrices and Freeness with Amalgamation, Int. Math. Research Notices **1996**, 1013 (1996).
 - [35] Y. V. Fyodorov, O. A. Chubykalo, F. M. Izrailev, and G. Casati, Wigner random banded matrices with sparse structure: local spectral density of states, Phys. Rev. Lett. **76**, 1603 (1996).
 - [36] M. Srednicki, The approach to thermal equilibrium in quantum chaotic systems, J. Phys. A **32**, 1163 (1999).
 - [37] Y. V. Fyodorov, private communication.
 - [38] F. J. Dyson, A Brownian-Motion Model for the Eigenvalues of a Random Matrix, J. Math. Phys. **3**, 1191 (1962).
 - [39] J. Richter, F. Jin, L. Knipschild, H. De Raedt, K. Michielsen, J. Gemmer, and R. Steinigeweg, Exponential damping induced by random and realistic perturbations, Phys. Rev. E **101**, 062133 (2020).
 - [40] K. Balzer, F. A. Wolf, I. P. McCulloch, P. Werner, and M. Eckstein, Nonthermal melting of Néel order in the Hubbard model, Phys. Rev. X **5**, 031039 (2015).
 - [41] Note that $1+J/L$ is a positive operator, so that its square root is well-defined.
 - [42] L. Vidmar and M. Rigol, Generalized Gibbs ensemble in integrable lattice models, J. Stat. Mech. **2016**, 064007 (2016).
 - [43] F. Igloi and H. Rieger, Long-Range Correlations in the Nonequilibrium Quantum Relaxation of a Spin Chain, Phys. Rev. Lett. **85**, 3233 (2000).
 - [44] J. Dziarmaga, Dynamics of a Quantum Phase Transition: Exact Solution of the Quantum Ising Model, Phys. Rev. Lett. **95**, 245701 (2005).
 - [45] T. Puškarov and D. Schuricht, Time evolution during and after finite-time quantum quenches in the transverse-field Ising chain, SciPost Phys. **1**, 003 (2016).
 - [46] D. Nickelsen and M. Kastner, Modelling equilibration of local many-body quantum systems by random graph ensembles, Quantum **4**, 273 (2020).
 - [47] S. Sugimoto, R. Hamazaki, and M. Ueda, Test of Eigenstate Thermalization Hypothesis Based on Local Random Matrix Theory, arXiv:2005.06379 (2020).
 - [48] L. Lorentzen and H. Waadeland, *Continued Fractions with Applications* (Elsevier North-Holland, Amsterdam, 1992).
 - [49] In the case $t = 0$, the condition (ii) below (20) may in general not be sufficient to guarantee the existence of the integral in (C3). [For instance, $|z G(z)| \rightarrow 0$ for $|z| \rightarrow \infty$ instead of (ii) would be sufficient. However, $G(z)$ often does not satisfy such a condition, as exemplified by the approximations (40) and (71).] Hence, the existence must be verified on a case by case basis. Alternatively, $t = 0$ may be tacitly excluded in (C3), and $g(0)$ is then given by (C5) rather than by (C1), see also the discussion below (C5).